September 1987 LIDS-P-1704

RECONSTRUCTING CONVEX SETS FROM SUPPORT LINE MEASUREMENTS *

Jerry L. Prince

Alan S. Willsky

Laboratory for Information and Decision Systems

Department of Electrical Engineering and Computer Science

Massachusetts Institute of Technology, Cambridge, MA 02139

September 9, 1987

Abstract

This paper proposes algorithms for reconstructing convex sets given noisy support line measurements. We begin by observing that a set of measured support lines may not be consistent with *any* set in the plane. We then develop a theory of consistent support lines which serves as a basis for reconstruction algorithms that take the form of constrained optimization algorithms. The formal statement of the problem and constraints reveals a rich geometry which allows us to include prior information about object position and boundary smoothness. The algorithms, which use explicit noise models and prior knowledge, are based on ML and MAP estimation principles, and are implemented using efficient linear and quadratic programming codes. Experimental results are presented. This research sets the stage for a more general approach to the incorporation of prior information concerning and the estimation of object shape.

*This research was supported by the National Science Foundation grant ECS-8312921 and the U.S. Army Research Office grants DAAG29-84-K-0005 and DAAL03-86-K-1071. In addition, the work of the first author was partially supported by a U.S. Army Research Office Fellowship.

I. Introduction

In this paper we consider algorithms for reconstructing 2-D convex sets given support line measurements for which the angles are known precisely but the lateral displacements are noisy. Our initial motivation for studying this problem was provided by a problem in computed tomography (CT) (see [1], for example). Specifically, in CT one makes measurements of integrals of an object property (absorption density) along various straight lines. As illustrated in Fig. 1, perfect measurement of a *projection* — i.e. of a full set of integrals along the parallel lines $L(t, \theta)$ with θ fixed — provides us knowledge of the two extreme lines at this angle that just graze the set on either side. These are known as ***support lines.*** Note that knowledge of these support lines in this case is completely equivalent to knowledge of the *silhouette* at this angle [2,3], i.e. to a function that is 1 if $L(t, \theta)$ intersects the object and 0 otherwise. Given such support lines from many different angles, it is possible to reconstruct a convex 2-D polyhedron, which contains the object, by intersecting all of the halfplanes defined by the measurements (since each support line also comes with information on which side of the line the object lies). When the projections are noisy, however, such as is the case in low-dose CT, then the estimates of the lateral positions of the support lines will also be noisy. In this case, the set of measured lines may be inconsistent — that is, taken together, there may be no set S which has all of the measured lines as support lines.

The consistency conditions on support lines, which will be discussed in detail later, form the basis of the algorithms presented in this paper. These algorithms use the consistency requirements, along with known noise statistics and prior information, to reconstruct a convex set which is in a specific sense the optimal estimate based on all the available information. In our work on CT, we have found that such knowledge of support — provided by a procedure of the type developed here — can assist dramatically in the problem of complete reconstruction, particularly when only limited data is available [4]. In this sense the work presented here can be viewed as a natural successor to that of Rossi and Willsky [5] and

Bresler and Macovski [6] who developed maximum likelihood (ML) methods for estimating parametric descriptions of objects in a CT cross section. In contrast to this previous work, we do not constrain objects to lie within specified parametric classes but rather use the fundamental properties of support lines to develop geometric reconstruction algorithms. This framework also allows us to incorporate prior information concerning object shape in a more flexible manner by specifying prior distributions on sets of support lines rather than by constraining objects to be simple shapes characterized by a few parameters.

It is also worth noting that the reconstruction problem considered in this paper is also of interest in a number of other applications. For example, in tactile sensing [7], a parallel plate robot jaw may provide two support line measurements as it clamps down on a "thick 2-D object" which is completely enclosed by the jaw. The jaw may then clamp down from different angles yielding a finite set of support line measurements, as in the CT example above. Other applications include robot vision [8] and chemical component analysis [9].

The problem described in this paper is fundamentally a problem in computational geometry [10], [11]. In contrast to most work in this field which assumes perfect measurements of information such as points, lines, and sets, and focuses on issues such as algorithm complexity, we focus explicitly on an estimation/optimization theoretic perspective so that we may deal with uncertain measurements and, where appropriate, incorporate prior knowledge. As we will see, the incorporation of measurement error statistics, prior knowledge, and the fundamental constraint on support lines can lead to optimization-based algorithms of considerable efficiency. Indeed the algorithms presented here are implemented with linear programming and quadratic programming methods, both useful tools in computational geometry.

The support line measurements we consider in this paper have known angles evenly spaced over 2π. In addition, we assume that a support line measurement consists not only of a lateral position, but also indicates on which side of the line the object lies. A natural first guess at a reconstruction then would be to intersect the halfplanes determined by each of the support lines. To see why this intersection method might not be a desireable reconstruction and also to give some insight into the fundamental support constraint, consider Fig. 2. Fig. 2(a) shows a set of six perfect support line measurements corresponding to the unit circle. The reconstruction resulting from the intersection method is the shaded hexagonal region which is obviously the best reconstruction given these measurements. Suppose now, however, that there are measurement uncertainties and in particular that all six lines have the lateral measurement errors indicated in Fig. 2(b). In this case, the intersection method produces the diamond shaped estimate indicated by the shaded region. Note that the two vertical lines on either side do not touch the diamond, and in fact, it should be apparent that given the other four measurements as indicated, there is *no* set that has these six lines as support lines. This demonstrates, geometrically, what is meant by inconsistency. Now consider what the diamond estimate implies about the noise model. What this estimate is telling us is that the two vertical lines (the outermost lines) are in error, and that the remaining four lines (the innermost lines) are perfect. Obviously, this does not correspond to any reasonable noise model, in general. The algorithms developed in this paper, in contrast to the intersection method, use explicit noise models to develop optimum methods given the model.

The paper is organized as follows. In Section II, we define the support vector and describe the fundamental support line constraints, i.e., the consistency conditions. In Section III we define the set of all consistent support vectors, called the support cone, and elaborate on the geometry of the support cone and of objects represented by points in this cone. Section IV presents the noise models and algorithms that use the geometry of the support cone to advantage, and Section V contains experimental results. We give concluding remarks in Section VI, including a brief discussion of how more elaborate models of prior shape information can be included.

II. Support Line Constraints

Support Lines and Support Functions

Fig. 3 shows what is meant by the support line $L_S(\theta)$ of a set S. It is the line orthogonal to the unit normal ω which just "grazes" S in the positive ω direction. The quantity $h(\theta)$ is the value of the largest possible projection of any point in S onto the ω-axis. One can see that S lies completely in a particular one of the two halfplanes determined by $L_S(\theta)$. We may now define the above quantities precisely. The *support line* at angle θ for the closed and bounded 2-D set S is given by

$$L_S(\theta) = \{x \in \mathbb{R}^2 \mid x^{\mathrm{T}}\omega = h(\theta)\} \tag{1}$$

where $\omega = [\cos\theta \quad \sin\theta]^{\mathrm{T}}$ and

$$h(\theta) = \sup_{x \in S} x^{\mathrm{T}}\omega \ . \tag{2}$$

The function $h(\theta)$ is called the *support function* of the set S; for any particular value of θ we call $h(\theta)$ the *support value* at angle θ.

The support function $h(\theta)$ has important and well-known properties which are analogous to properties we shall be developing for the support vector defined below (see [12], [13], and [14]). For example, $h(\theta)$ uniquely determines the convex hull of S, $\mathrm{hul}(S)$. It is also true that if $h(\theta)$ is twice differentiable then S itself must be convex, and the boundary of S must be continuous and smooth (i.e., it has continuously turning normals). In this case, the curvature of the boundary of S at the boundary point $e(\theta) = L_S(\theta) \cap S$ (see Fig. 3) is given by $h''(\theta) + h(\theta)$. Then, since S is convex, the curvature of its boundary must be non-negative, which leads to the conclusion that support functions which are twice differentiable must satisfy the constraint

$$h''(\theta) + h(\theta) \geq 0 \ . \tag{3}$$

The constraint we derive below is analogous to (3), but is more fundamental since it applies to *any* set in the plane, not just convex sets with smooth boundaries. We shall also develop an analog to the radius of curvature which will be exploited by algorithms designed to incorporate prior knowledge.

Support Vectors and Constraints

We shall require some additional notation in this section. From this point on, we consider a finite number M of angles $\theta_i = 2\pi(i-1)/M$, $i = 1, \ldots, M$, spaced evenly over $[0, 2\pi)$, and associated sets of lines L_i, orthogonal to the corresponding unit vector $\omega_i = [\cos\theta_i \;\; \sin\theta_i]^{\mathrm{T}}$. In what follows the index i is always interpreted modulo M. The line L_i is defined by its lateral displacement h_i, via

$$L_i = \{u \in \mathbb{R}^2 \mid u^{\mathrm{T}}\omega_i = h_i\} \tag{4}$$

The most important quantity in this paper is the vector made by organizing the M lateral displacement values of the M lines under consideration as a vector $h = [h_1 \; h_2 \; \ldots \; h_M]^{\mathrm{T}}$. We call the vector h a *support vector* if the lines L_i, for $i = 1, \ldots, M$ are support lines for some set $S \in \mathbb{R}^2$, i.e. if $h_i = h(\theta_i)$ where $h(\theta)$ is the support function of some set S. In this case we refer to the h_i as *support values.*

Before proceeding to the basic theorem of this paper, let us characterize, in terms of the quantities defined above, the estimate produced by the intersection method introduced in Section I. Given measurements h_i, $i = 1, \ldots, M$ of the lateral displacements of M lines, the intersection method simply produces the set of all points $u \in \mathbb{R}^2$ which satisfy $u^{\mathrm{T}}\omega_i \leq h_i$ for all $i = 1, \ldots, M$, i.e.[1]

$$S_B \;\; = \;\; \{u \in \mathbb{R}^2 \mid u^{\mathrm{T}}[\omega_1 \, \omega_2 \, \ldots \, \omega_M] \leq [h_1 \, h_2 \, \ldots \, h_M]\} \; . \tag{5}$$

The two shaded regions in Fig. 2 correspond to S_B for two different vectors h. In Fig. 2(a), h is a support vector since the lines actually support S_B, however in Fig. 2(b), h is not a support vector because there is no set which the given lines support. We now proceed

[1] A vector inequality such as $x^{\mathrm{T}} \leq y^{\mathrm{T}}$ where $x, y \in \mathbb{R}^n$ implies that $x_i \leq y_i$ for $i = 1, \ldots, n$, where x_i and y_i are the i^{th} elements of the vectors x and y respectively.

to state the basic theorem of this paper, which characterizes precisely the consistency constraints satisfied by support vectors.

Theorem 1 (The Support Theorem)

A vector $h \in \mathbb{R}^M$ $(M \geq 5)$ *is a support vector if and only if*

$$h^{\mathrm{T}} C \leq [0 \ldots 0] \tag{6}$$

where C *is an* M *by* M *matrix given by*

$$C = \begin{bmatrix} 1 & -k & 0 & & & -k \\ -k & 1 & -k & \ldots & \ldots & 0 \\ 0 & -k & 1 & & & \vdots \\ \vdots & 0 & -k & \ldots & \ldots & 0 \\ 0 & \vdots & & & & -k \\ -k & 0 & 0 & & & 1 \end{bmatrix} \tag{7}$$

and $k = 1/(2\cos(2\pi/M))$. □

It is important to point out the similarity between the continuous support function constraint of (3) and the the discrete support vector constraint of (6). The quantity $-h^{\mathrm{T}}C$, which has *non-negative* entries, is analogous to the quantity $h''(\theta) + h(\theta)$, which is also non-negative. It can be shown, in fact, that in the limit as $M \rightarrow \infty$ the expression $-h^{\mathrm{T}}C \geq 0$ goes to $h''(\theta) + h(\theta) \geq 0$ [15]. As a further extension of the analogy, we shall reveal in a subsequent section that the entries of the vector $-h^{\mathrm{T}}C$ can be directly interpreted from the geometry as a type of discrete radius of curvature. This interpretation allows us to propose methods for incorporating prior shape information related to boundary smoothness in the algorithms of Section III.

Before proceding with the proof, we give a brief indication of the geometric intuition behind it. First, consider the situation depicted in Fig. 4, in which we have shown two lines L_{i-1} and L_{i+1}. A third line L_i is parallel to the dashed line in the figure, and we seek constraints on the lateral displacement of this line so that the 3 lines L_{i-1}, L_i, and L_{i+1} could possibly be support lines of some set. If L_{i-1} and L_{i+1} are support lines of a set S, then S is contained in the set D_i illustrated in the figure. Now suppose that the line L_i were located to the left of (and parallel to) the dotted line. Then it is possible to construct a set $S \subset D_i$ which touches each of the three lines L_{i-1}, L_i, and L_{i+1} — these lines are consistent. However, if L_i were measured to the right of the dotted line, then it is impossible to construct such a set — these lines are inconsistent. When stated in mathematical notation and applied to all lines L_i, $i = 1, \ldots, M$, this relationship yields precisely the vector constraint in (6).

The above observation leads to the necessity of (6), but in order to establish the sufficiency of (6) we need to define a new set $S_\nu \in \mathbb{R}^2$ which may be thought of as another choice of reconstruction, different than S_B. As shown in Fig. 5, S_ν is formed from the convex hull of the points of intersection of lines L_i and L_{i+1} for $i = 1, \ldots, M$. Formally, we have that

$$S_\nu \quad = \quad \text{hul}(\nu_1, \nu_2, \ldots, \nu_\text{M}) \tag{8}$$

where the ν_i's are given by

$$\nu_i = L_i \cap L_{i+1} \tag{9}$$

and hul(.) denotes the convex hull. We refer to the points ν_i as ***vertex points*** rather than vertices because, as one can see from Fig. 5(b), they need not be distinct points. In Fig. 5(a) the support line L_1 is located to the right of the point $L_2 \cap L_5$, and from our discussion on Fig. 4, we know that these lines do not satisfy (6). Note that in this case $S_B \neq S_\nu$. However, in Figs. 5(b) and 5(c) the lines do satisfy (6) and $S_B = S_\nu$. Indeed what we show in the proof is that (6) implies that $S_B = S_\nu$ and h is the support vector to this set.

Proof of Theorem 1:

First, we show the necessity of condition (6). By hypothesis, h is a support vector of some set S. Now consider the set D_i defined by the two support lines L_{i-1} and L_{i+1} as shown in Fig. 4. Note that by hypothesis $M \geq 5$, which implies that $\theta_{i+1} - \theta_{i-1} < \pi$. This in turn implies that the two lines L_{i-1} and L_{i+1} have a finite intersection point p_i (see Fig. 4), and that ω_i may be written as a positive combination of ω_{i-1} and ω_{i+1}. These two facts are necessary and in fact easily allows us to conclude that the support value at angle θ_i for the set D_i is $p_i^{\mathrm{T}}\omega_i$. Then, since $S \subset D_i$ we must have that $h_i \leq p_i^{\mathrm{T}}\omega_i$. With some algebraic manipulation (see Appendix A), this inequality may be shown to be equivalent to the condition given by the i^{th} column of (6).

To prove the sufficiency of (6) we must show that a vector h which satisfies (6) is a support vector for some set. In Appendix B we show that (6) implies that $S_B = S_\nu = S$, and what remains then is to show that S has h as its support vector. To see this, first note from the definition of S_B in (5), that we must have

$$\sup_{x \in S} x^{\mathrm{T}}\omega_i \leq h_i.$$

On the other hand, $\nu_i \in S_\nu = S_B = S$ and $\nu_i^{\mathrm{T}}\omega_i = h_i$. Consequently, h_i is the support value at this angle. □

The immediate use of the support theorem is as a test of consistency. Given a test vector h we may determine whether h specifies a consistent set of support lines by evaluating $h^{\mathrm{T}}C$ and seeing whether the elements of the resultant row vector are all non-positive. From an estimation viewpoint, we see that if we are trying to estimate a support vector h from a set of noisy measurements, then we must make sure that our estimate $\hat{h}$ satisfies $\hat{h}^{\mathrm{T}}C \leq 0$. In the following section we examine the geometry of these constraints in more detail.

III. Object and Support Cone Geometry

Geometry of the Support Cone

The convex polyhedral cone given by

$$\mathcal{C} = \{h \in \mathrm{IR}^M \mid h^{\mathrm{T}}C \leq [0\ldots0]\} \tag{10}$$

consists of all M-dimensional support vectors. We call $\mathcal{C}$ the *support cone.*[2] The matrix C is circulant and, therefore, its eigenvalues are given by the discrete Fourier transform of the first row [16]. After simplification (see Appendix A), the eigenvalues are found to be

$$\lambda_k = 1 - \frac{\cos(2\pi(k-1)/M)}{\cos(2\pi/M)} \quad k = 1, \ldots, M.$$

We now recognize that exactly two eigenvalues are identically zero: $\lambda_2 = \lambda_{\mathrm{M}} = 0$. Hence, C is singular, and a basis for the nullspace $\mathcal{N}$ (and also of the left nullspace since C is symmetric), is found to be

$$\begin{aligned} n_1 &= \begin{bmatrix} 1 & \cos\theta_o & \cos 2\theta_o & \ldots & \cos(\mathrm{M}-1)\theta_o \end{bmatrix}^{\mathrm{T}} \\ n_2 &= \begin{bmatrix} 0 & \sin\theta_o & \sin 2\theta_o & \ldots & \sin(\mathrm{M}-1)\theta_o \end{bmatrix}^{\mathrm{T}} \end{aligned} \tag{11}$$

where $\theta_0 = 2\pi/M$.

The geometrical consequence of C being singular is that the support cone $\mathcal{C}$ is not a proper cone; i.e., there is a linear subspace (of dimension 2) contained entirely in $\mathcal{C}$. Therefore, the support cone is composed of the Cartesian product of a proper cone, $\mathcal{C}_p = \{h \in \mathcal{C} \mid h^{\mathrm{T}} n_1 = 0,\ h^{\mathrm{T}} n_2 = 0\}$, and $\mathcal{N}$, the nullspace of C. Accordingly, any support vector may be written as the sum of two orthogonal components, h_p and h_n, as

$$h = h_p + h_n \tag{12}$$

where $h_p \in \mathcal{C}_p$ and $h_n \in \mathcal{N}$. We will see in the following section that the nullspace component of a support vector h may be interpreted as a simple *shift* of the set in the plane that corresponds to h.

Object Geometry

Given a (consistent) support vector h, there are, in general, an entire family of sets which have h as their support vector. The largest of these sets, which is uniquely determined by

[2] $\mathcal{C}$ is a cone because it obeys the usual property of cones: if h is in $\mathcal{C}$ then αh ($\alpha > 0$) is also in $\mathcal{C}$. It is a polyhedron because it is the intersection of a finite number of closed half spaces in $\mathbb{R}^M$.

h is the polygonal set S_B defined in (5). We call S_B the *basic object* of support vector h. Two examples of basic objects for $M = 5$ are shown in Figs. 5(b) and 5(c). Note that for M small, S_B may not be a good approximation to the true set S, but as M gets larger, S_B becomes an increasingly better approximation to hul(S).

Suppose we were to add a nullvector h_n to support vector h. What happens to the basic object? We show here that it is simply *shifted* (or translated) in the plane. We start by noting that any nullvector may be written as

$$h_n = Nv \tag{13}$$

where

$$N = [n_1 \; n_2] \tag{14}$$

(see (11)) and v is a two-dimensional vector. Next, we notice that S_B may be written as

$$S_B = \{u \in \mathbb{R}^2 \mid u^{\mathrm{T}} N^{\mathrm{T}} \leq h^{\mathrm{T}}\} \quad .$$

Now suppose that w is an element of S_B; then, clearly, w satisfies

$$h \geq Nw \quad . \tag{15}$$

Now we may add, component by component, equations (13) and (15) (preserving the inequality) yielding

$$h + h_n \geq N(w + v) \quad .$$

Finally, we now see that $w + v$ must be an element of the basic object corresponding to $h + h_n$, i.e., the new basic object is just a shifted version of S_B. Clearly, the reverse holds as well: shifting S_B by v corresponds to adding the nullvector Nv to h.

The extreme points of the basic object, which we have termed vertex points, are given by the points $\nu_1, \ldots, \nu_M$ in (9) (see Figs. 5(b) and 5(c)). An explicit equation for the vertex point ν_i is easily found using the definition of L_i and L_{i+1} and solving a system of two linear equations (see Appendix A). We find that

$$\nu_i^{\mathrm{T}} = \frac{1}{\sin\theta_o} \begin{bmatrix} h_i & h_{i+1} \end{bmatrix} \begin{bmatrix} \sin\theta_{i+1} & -\cos\theta_{i+1} \\ -\sin\theta_i & \cos\theta_i \end{bmatrix} \quad i = 1, \ldots, M \ . \tag{16}$$

where $\theta_o = \theta_{i+1} - \theta_i = 2\pi/M$. The "shift" property given above relates to the *relative* position of two identically-shaped and oriented basic objects. It turns out that a useful definition of the *absolute* position of a basic object is the average position of its vertex points, denoted $\bar{\nu}$. The relationship between the support vector h and $\bar{\nu}$ is found to be (see Appendix A)

$$\bar{\nu} = \begin{bmatrix} \bar{\nu}_x \\ \bar{\nu}_y \end{bmatrix} = \frac{1}{\mathrm{M}} \sum_{i=1}^{\mathrm{M}} \nu_i = \frac{2}{\mathrm{M}} N^{\mathrm{T}} h \ . \tag{17}$$

We shall see in Section IV that (17) can be used as a constraint on estimated support vectors if the position of the true object is known *a priori*. Note, in particular, that when h has no nullspace component, i.e., h is in $\mathcal{C}_p$, then $N^{\mathrm{T}}h = 0$ and, therefore, $\bar{\nu} = 0$ — the basic object is centered on the origin.

Now we develop the idea of "discrete radius of curvature" to characterize the smoothness of the boundaries of basic objects. Suppose that in Fig. 4, the line L_i were to pass through the intersection point p_i of L_i and L_{i+1}. Then the boundary of S_B is "sharp" at that point. As L_i moves toward the left of p_i, the boundary is made "smoother". Now consider the more detailed drawing in Fig. 6. As the boundary is traced along the i^{th} face from ν_{i-1} to ν_i, the outward unit normal to the boundary changes in angle by $\theta_0 = \theta_i - \theta_{i-1}$ over a distance f_i. In analogy to the usual radius of curvature, which is defined as the rate of change of arclength with respect to the angle the unit normal makes to the x-axis, we define the i^{th} *discrete radius of curvature* as

$$r_i = \frac{f_i}{\theta_0} \ . \tag{18}$$

It can be shown from the geometry (see Appendix A) that the distance from p_i to L_i is given by $\rho_i = -h^{\mathrm{T}}c_i$, where c_i is the i^{th} column of C. Then, by simple trigonometry, we have that

$$f_i = \frac{2\rho_i}{\tan\theta_0} \tag{19}$$

and, hence

$$\rho_i = \frac{1}{2} r_i \theta_0 \tan\theta_0 \tag{20}$$

Hence, the vector $\rho = -h^{\mathrm{T}}C$ has elements that are proportional to the discrete radii of curvature, r_i. The elements of ρ which are small correspond to "sharp" corners; the larger elements correspond to "smoother" boundaries. We use this idea in Section IV to incorporate prior knowledge about object shape.

This completes the discussion of geometry of the support cone and basic objects. Using the constraints established in Section II and the geometrical ideas established in this section, we proceed to develop algorithms for estimating support vectors (and hence the basic objects) given noisy observations. The geometrical ideas play a role both in the development of prior information to be included in the statement of the algorithms, and in the execution and analysis of the actual computational methods.

The algorithms we develop in the following section are constrained optimization algorithms because the support vectors to be estimated are constrained to lie in the support cone. Fortunately, the constraints are linear inequalities, which are simple enough to allow efficient computational methods. A further constraint which may be imposed if the position of the object is known a priori, is a linear equality constraint, which is even simpler. The algorithms are designed to illustrate how to incorporate these constraints along with prior information and noise models to reconstruct convex sets. We have elected to demonstrate only the simplest formulations necessary to accomplish this goal. As a result, the algorithms use the very efficient computational methods of linear programming (LP) and quadratic programming (QP). In Section VI, we discuss possible extensions which include more sophisticated models of prior information and that will undoubtedly lead to somewhat more complex algorithms.

IV. Estimation Algorithms

We now present three estimation algorithms based on the ideas developed in Sections II and III. We assume that the measured support values are given by

$$y_i = h_i + n_i, \quad i = 1, ..., \mathrm{M} \tag{21}$$

where h_i are the true support values which we are estimating and n_i are samples of either 1) independent white Gaussian noise with zero mean and variance σ^2, or 2) uniformly distributed noise over the range $[-\gamma, \gamma]$. Because of the noise, it is likely that the measurement vector $y = [y_1 \ \ldots, \ y_M]^{\mathrm{T}}$ is not a feasible support vector. Therefore, the first objective of the following algorithms is to obtain a feasible support vector from the measurements. The second objective is to use prior information to guide the estimates toward "preferable" values. The development begins with the Closest algorithm, which uses a minimum of prior knowledge in a maximum likelihood (ML) formulation, and concludes with the Close-Min algorithm, which uses prior shape information in a formulation much like maximum *à posteriori* (MAP) estimation. The algorithms also tend to increase in complexity as we proceed, but are each solved by efficient quadratic or linear programming methods.

The Closest Algorithm

Here, we assume the Gaussian noise model given above. In the absence of any prior probabalistic knowledge we may form the maximum likelihood estimate of h given the measurement vector y and subject to $h \in \mathcal{C}$ as (see, for example, [17])

$$\hat{h}_C = \hat{h}_{ML} = \underset{h:\, h^{\mathrm{T}}C \leq 0}{\operatorname{argmax}} \ -\frac{1}{2}(y-h)^{\mathrm{T}}(y-h) \ . \tag{22}$$

We see that this estimate is the support vector h in $\mathcal{C}$ which is *closest* (in the Euclidean metric) to the observation y. If y is in $\mathcal{C}$ then $\hat{h}_C = y$, otherwise the solution may be found by (efficient) quadratic programming (QP) methods (see, for example, [18] and [19]).

The Mini-Max Algorithm

The Mini-Max algorithm incorporates the following prior knowledge: objects of interest tend to have smooth boundaries. To cause objects to have smooth boundaries we define the Mini-Max estimate to *maximize the minimum discrete radius of curvature.* As the problem is stated, however, the solution is unbounded, since basic objects circumscribing circles of ever increasing radii have unbounded discrete radii of curvature. This problem is partially solved by incorporating the uniform noise model. In this case, since the noise is bounded by $\pm\gamma$, each element of the true solution cannot be farther than γ away from the corresponding element of the observation. Formally, we write that the true vector, and therefore the estimate, must be an element of the hypercube

$$\mathcal{B} = \{h \in \mathbb{R}^M \mid y - [\gamma\,\gamma\,\ldots\,\gamma]^{\mathrm{T}} \leq h \leq y + [\gamma\,\gamma\,\ldots\,\gamma]^{\mathrm{T}}\} \tag{23}$$

Finally, recognizing that the estimate must also be in the support cone, and recalling the proportionality of $\rho_i = -h^{\mathrm{T}} c_i$ to the discrete radius of curvature r_i (see (20)), we define the Mini-Max estimate as

$$\hat{h}_{MM} = \underset{h:\, h \in \mathcal{C} \cap \mathcal{B}}{\operatorname{argmax}}\ \min\{-h^{\mathrm{T}}c_1,\ -h^{\mathrm{T}}c_2,\ \ldots,\ -h^{\mathrm{T}}c_M\} \tag{24}$$

where $c_1, \ldots, c_M$ are the columns of C.

The solution to (24) may be found by linear programming (LP) techniques (see [20], for example). To show that this is so, we define a new scalar variable μ which satisfies

$$\mu \leq -h^{\mathrm{T}} c_i \quad i = 1, \ldots, M\ . \tag{25}$$

Now consider the two augmented vectors

$$u = \begin{bmatrix} h \\ \\ \mu \end{bmatrix} \quad \text{and} \quad b = \begin{bmatrix} 0 \\ \\ 1 \end{bmatrix}\ . \tag{26}$$

We now notice that the solution to (24) may be found by maximizing $u^{\mathrm{T}}b$, subject to the original constraints and the new constraints given in (25). The new objective function is clearly linear in u; and both sets of constraints are linear in u. Therefore, the augmented problem is an LP and may be solved by any LP code, or a QP code with the Hessian matrix set to zero.

Unfortunately, as is often true of LP's, the solution to (24) may not be unique. We may see a potential non-uniqueness by observing that adding a vector from the nullspace of C does not change the value of the objective function. Therefore, providing that the constraints are still met, there may be a family of shifted objects, each one corresponding to an optimal solution to (24). The Mini-Max estimate is also tied to the observations only by the hypercube $\mathcal{B}$, and as γ (and therefore the size of $\mathcal{B}$) increases, the influence of the measurements on the solution may decrease dramatically. For example, we expect that the basic object corresponding to the estimate resulting from this objective function will be as largest possible given the bounds, and as near to circular as possible so as to maximize the minimum discrete radius of curvature. Thus, even if the true object is quite eccentric, and the observation is just barely infeasible, the Mini-Max estimate may resemble a circle if the bound γ is large. We shall see examples of both types of behavior in Section V. In addition, these observations provided part of the motivation for the next algorithm.

The Close-Min Algorithm

The Close-Min algorithm is designed to combine the Closest and Mini-Max algorithms to produce an estimate which attempts to match the observations, as in the Closest algorithm, yet also incorporate prior knowledge, as in the Mini-Max algorithm. The concept is simple: we define a new cost function which is a convex combination of the two objective functions. We note that this method resembles MAP estimation where the Closest objective function plays the role of the logarithm of the measurement density (assuming the Gaussian model), and the Mini-Max objective function plays the role of the logarithm of the prior density.

The trade-off between these two objective functions is controlled by the parameter α which has a value between 0 and 1. This provides the means for weighting prior information and that available from the measurements as is done in optimal MAP estimation.

The Close-Min estimate is defined as

$$\hat{h}_{CM} = \underset{h:\ h \in \mathcal{C} \cap \mathcal{B}}{\operatorname{argmax}}\ \alpha f_C(h) + (1-\alpha) f_M(h) \tag{27}$$

where $0 \leq \alpha \leq 1$ and

$$\begin{aligned} f_C(h) &= -\frac{1}{2}(y-h)^{\mathrm{T}}(y-h) \\ f_M(h) &= \min\{-h^{\mathrm{T}}c_1,\ -h^{\mathrm{T}}c_2, \ldots, -h^{\mathrm{T}}c_M\} \end{aligned}$$

are the objective functions corresponding to the Closest and Mini-Max algorithms, respectively. The solution to (27) may be found using QP after augmenting h as in (26). Note that provided $\alpha \neq 0$, the constraint $\mathcal{B}$ may be removed and the solution will be unique.

Shift Corrected Algorithms

As we suggested previously, prior positional information may be included in the estimation process. Suppose one knows that the true object is centered at $\bar{\nu}$, that is, that the average position of its vertex points is $\bar{\nu}$. Then the estimate should also be centered at $\bar{\nu}$. From Equation (17) we see that this may be assured provided that we enforce the following linear constraint

$$N^{\mathrm{T}}h = \frac{M}{2}\bar{\nu} \tag{28}$$

Since this is a linear equation, (28) may be incorporated into the three algorithms as an additional linear constraint causing no essential change in the nature of the solution method. The effect of this added prior knowledge can be quite dramatic, however, as we shall see in the following section.

V. Experimental Results

To show the behavior of the three algorithms, we use noise-corrupted measurements of a 10-dimensional support vector corresponding to either 1) a circle with radius 1/2, centered on the origin or, 2) an ellipse, also centered on the origin, with major axes in the x-direction with radius 3/4 and y-direction with radius 1/3. The measurements are given by (21) where n_i are independent random variables, uniform over the range $[-\gamma, \gamma]$, with several values of γ. To plot the data (for either the feasible support vectors or infeasible observations) we simply connect the vertex points $\{\nu_1, \nu_2, \ldots, \nu_M, \nu_1\}$ in sequence, producing a *vertex plot.* For a (feasible) support vector, this plot produces an outline of the basic object; however, for a (infeasible) measurement, the plot crosses itself, clearly demonstrating the infeasibility. We refer to a point where a vertex plot crosses itself as a *point of inconsistency.*

Figs. 7(a) and 8(a) show both the true basic object corresponding to the circle (dashed line) and the vertex plot for the measured vector (solid line), where $\gamma = 0.2$ and $\gamma = 0.4$, respectively. Figs. 9(a) and 10(a) show the corresponding figures for the ellipse. The shaded regions shown in the (a) panels of Figs. 7–10 are estimates produced by the intersection method which is described in Sections I and II. One can see that, in each case, there is at least one measured line which does not support the shaded region, which clearly demonstrates the infeasibility of the measurements. It is important to point out that the set constructed from the raw measurements using the intersection method is a bad estimate of the true set, in general. This is because, as mentioned before, the construction of this set essentially ignores the support lines that are farthest out. In contrast, each of the algorithms proposed here uses *all* of the measurements to "pull" the inner support lines out, if necessary.

In panels (b)–(d) of Figs. 7–10, the shaded regions correspond to the estimated basic objects produced by the three algorithms using the measurements shown in the respective (a) panels. The results of the Closest algorithm are shown in the (b) panels, the Mini-Max algorithm in the (c) panels, and the Close-Min algorithm in the (d) panels. For comparison, we have also included the outline of the true basic object (dashed line) in each of these panels. The most important observation to make here is that the Closest estimates strongly resemble the measurements, the Mini-Max estimates strongly resemble our prior expectation (large circular objects) and the Close-Min estimates "blend" these two outcomes. Note that we have chosen $\alpha = 0.5$ for the Close-Min experiments; clearly, there are a range of different estimates corresponding to different α's which should yield figures ranging between the Closest and Mini-Max solutions.

Let us examine the results in more detail. The Closest estimates show the following behavior: the lines are moved just enough in order to correct the points of inconsistency. Note that, around a point of inconsistency, the inner lines are "pulled" out and the outer lines are "pushed" in. This is in accordance with the Closest criteria which, in words, is to adjust the lateral positions of the lines in order to make them consistent, but in such a way that minimizes the sum of the squares of the lateral movements. For example, in Fig. 7(b) we see that three lines were moved to correct the single point of inconsistency. Note that it is possible to move only one line to fix such a point, but clearly that move yields a larger squared difference between observation and support vector. Because of this behavior, the Closest estimate always produces a basic object which is larger than the intersection method (provided that the measurement is infeasible). Then, for almost all noise models, we expect that the Closest estimate is better than the intersection method, since it is not as biased toward small figures.

To clarify some of the behavior of the Mini-Max estimates, it is useful to examine the estimates together with the bounds imposed by the hypercube $\mathcal{B}$ of (23). Fig. 11 shows the vertex plots for the Mini-Max estimate (solid line), the inner bound $y_a = y - [\gamma\,\gamma\,\ldots\,\gamma]^{\mathrm{T}}$ (dotted line), and the outer bound $y_b = y + [\gamma\,\gamma\,\ldots\,\gamma]^{\mathrm{T}}$ (dashed line) for the example shown in Fig. 7. First, this figure demonstrates how the Mini-Max estimate, in effort to maximize the minimum discrete radius of curvature, produces a figure which is as large as possible given the bounds, yet is also nearly circular (that is, nearly a regular polygon). Second, it is clear from the figure that the estimated basic object may be shifted down a short distance and still remain within the bounds. Since, as we have already pointed out, adding a nullvector to the estimated support vector does not affect the value of the Mini-Max objective function, any feasible shifted version of the solution is also optimal. Therefore, in this example, the solution is not unique. In the shift-corrected algorithms discussed below, this component of non-uniqueness is eliminated by imposing a known object position. As we shall see, this simple correction has dramatic effects on the Mini-Max estimates.

The Close-Min algorithm produced the "blended" estimates that we expected. In particular, where the Closest algorithm corrected the points of inconsistency, it invariably left a sharp corner on the boundary. The Close-Min algorithm produced estimates which appear quite similar to the results of the Closest algorithm but which have smoothed these corners.

Finally, we present one experiment which demonstrates the results of shift correction applied to the Mini-Max algorithm. Fig. 12 shows three vertex plots corresponding to the true support vector (solid line), the Mini-Max estimate from Fig. 7(c) (dotted line), and the Mini-Max shift-corrected (for $\bar{\nu} = 0$) estimate (dashed line). We see that the shift correction *does not simply shift the original Mini-Max solution down.* To understand this we recall Fig. 11. We saw that due to non-uniqueness we could shift the solution vertically over a finite range. But, evidently, none of these shifted positions causes the sum of the vertex points to be exactly zero. To allow this to occur, the shift-corrected algorithm was forced to shrink the estimate as well. Clearly, prior information about the position of the object may have a very strong influence on the performance of the algorithms.

VI. CONCLUSIONS

In this paper we have introduced several important ideas related to the reconstruction of convex sets from support line measurements. The primary contribution of this paper is in the formulation of the problem as a constrained optimization problem which includes the fundamental support vector constraint, prior information, and uncertainty in the measurements. We have shown how knowledge of

1. Fundamental geometric constraints,

2. Object shape and position, and

3. Underlying measurement noise models,

may lead directly to optimization-based or probabilistic-based algorithm formulations. We have shown how these methods produce better reconstructions, which are more consistent with the available information, than the conventional intersection method, which does not use any of this information.

The algorithms we have proposed in this paper are of the very simplest type, however, they serve the purpose of illustration of the fundamental ideas, and they are implemented using particularly efficient codes. The Closest algorithm gives the constrained maximum likelihood estimate assuming the noise is Gaussian. It requires the minimum amount of prior knowledge about the set to be reconstructed, and is implemented in a straightforward manner using quadratic programming techniques. The Mini-Max algorithm gives one method to produce smoother boundaries which results in fast linear programming codes. However, the Mini-Max solution is not necessarily unique and tends to produce large, nearly circular objects. The Close-Min algorithm blends the preceding two objective functions to produce estimates that balance the prior information and the information contained in the measurements. Finally, we have shown that prior knowledge of object location can lead to considerable improvement for the resulting shift-corrected algorithms. Note that object location is one quantity that can typically be estimated with great accuracy in CT applications.

Many extensions of this work are possible, both in the inclusion of additional constraints or in the development of more elaborate objective functions. Among the possible constraints one might consider including is a known object area. The area of a basic object is a quadratic function of h, however, which leads to inherently more complicated computational methods. A simpler extension of the constraints may arise if one has only partial information about the position of the object in the plane. For example, if the position were bounded, then instead of having two linear *equality* constraints (corresponding to the x and y position) as in the shift-corrected algorithms, one would have four linear *inequality* constraints.

A potentially important extension of the form of the objective function involves the development of explicit prior probabilities on support vectors. For example, if one interprets the Close-Min algorithm as an explicit MAP formulation, one finds that the implied prior distribution on h strongly favors large objects. This, in general, is not desirable. One would prefer to specify a prior distribution which permits separate control of size and smoothness, for example, and perhaps also makes explicit such quantities as eccentricity and orientation. Once specifying such prior distributions, the algorithms may be formulated precisely using MAP techniques with the additional knowledge of the measurement noise statistics. Results along these lines will be reported in a subsequent paper.

Another extension of these methods may be made to account for situations where one has missing measurements. This application is particularly important to the CT problem mentioned in Section I in the case when one has limited-angle or sparse-angle observations. For example, suppose one has M measurements but wishes to reconstruct a support vector of dimension $2M$. One may think of this as an interpolation or extrapolation procedure, and provided there is some prior shape information, this may be accomplished with relatively simple additions to the current algorithms [15].

A. FORMULAS

We collect here for convenience several formulas and brief derivations that are often referred to in the text. Here $\theta_0 = 2\pi/M$.

The point p_i of intersection of L_{i-1} and L_{i+1} (see Fig. 4):

$$\begin{aligned}
p_i^{\mathrm{T}} &= \begin{bmatrix} h_{i-1} & h_{i+1} \end{bmatrix} \begin{bmatrix} \omega_{i-1} & \omega_{i+1} \end{bmatrix}^{-1} \\
&= \begin{bmatrix} h_{i-1} & h_{i+1} \end{bmatrix} \begin{bmatrix} \cos\theta_{i-1} & \cos\theta_{i+1} \\ \sin\theta_{i-1} & \sin\theta_{i+1} \end{bmatrix}^{-1} \\
&= \frac{1}{\sin 2\theta_0} \begin{bmatrix} h_{i-1} & h_{i+1} \end{bmatrix} \begin{bmatrix} \sin\theta_{i+1} & -\cos\theta_{i+1} \\ -\sin\theta_{i-1} & \cos\theta_{i-1} \end{bmatrix}
\end{aligned}$$

Also

$$\begin{aligned}
p_i^{\mathrm{T}}\omega_i &= \frac{1}{\sin 2\theta_0} \begin{bmatrix} h_{i-1} & h_{i+1} \end{bmatrix} \begin{bmatrix} \sin\theta_{i+1} & -\cos\theta_{i+1} \\ -\sin\theta_{i-1} & \cos\theta_{i-1} \end{bmatrix} \begin{bmatrix} \cos\theta_i \\ \sin\theta_i \end{bmatrix} \\
&= \frac{1}{\sin 2\theta_0} \begin{bmatrix} h_{i-1} & h_{i+1} \end{bmatrix} \begin{bmatrix} \sin\theta_0 \\ \sin\theta_0 \end{bmatrix} \\
&= \frac{1}{2\cos\theta_0} (h_{i-1} + h_{i+1})
\end{aligned}$$

Since $h_i \leq p_i^{\mathrm{T}}\omega_i$, we see that this result yields the necessary result in Theorem 1.

Discrete radius of curvature:

$$\begin{aligned}
\rho_i &\equiv -h^{\mathrm{T}} c_i \\
&= \frac{1}{2\cos\theta_0} (h_{i-1} + h_{i+1}) - h_i \\
&= p_i^{\mathrm{T}}\omega_i - h_i
\end{aligned}$$

Vertex points:

$$\begin{aligned}
\nu_i^{\mathrm{T}} &= \begin{bmatrix} h_i & h_{i+1} \end{bmatrix} \begin{bmatrix} \omega_i & \omega_{i+1} \end{bmatrix}^{-1} \\
&= \begin{bmatrix} h_i & h_{i+1} \end{bmatrix} \begin{bmatrix} \cos\theta_i & \cos\theta_{i+1} \\ \sin\theta_i & \sin\theta_{i+1} \end{bmatrix}^{-1} \\
&= \frac{1}{\sin\theta_0} \begin{bmatrix} h_i & h_{i+1} \end{bmatrix} \begin{bmatrix} \sin\theta_{i+1} & -\cos\theta_{i+1} \\ -\sin\theta_i & \cos\theta_i \end{bmatrix}
\end{aligned}$$

Eigenvalues of the constraint matrix:

$$\begin{aligned}
\lambda_k &= \sum_{n=1}^{M} c_{1n} e^{-j2\pi(k-1)(n-1)/M} \quad k = 1, \ldots, M \\
&= 1 + \frac{-1}{2\cos 2\pi/M} e^{-j2\pi(k-1)/M} + \frac{-1}{2\cos 2\pi/M} e^{-j2\pi(k-1)(M-1)/M} \\
&= 1 - \frac{\cos 2\pi(k-1)/M}{\cos 2\pi/M}
\end{aligned}$$

The x and y coordinates of the center of gravity of the vertex points:

$$\begin{aligned}
\bar{v}_x &= \frac{1}{M} \sum_{i=1}^{M} \frac{1}{\sin\theta_0} \begin{bmatrix} h_i & h_{i+1} \end{bmatrix} \begin{bmatrix} \sin\theta_{i+1} \\ -\sin\theta_i \end{bmatrix} \\
&= \frac{1}{M\sin\theta_0} (h^{\mathrm{T}} \begin{bmatrix} \sin\theta_2 \\ \sin\theta_3 \\ \vdots \\ \sin\theta_M \\ \sin\theta_1 \end{bmatrix} - h^{\mathrm{T}} \begin{bmatrix} \sin\theta_M \\ \sin\theta_1 \\ \vdots \\ \sin\theta_{M-2} \\ \sin\theta_{M-1} \end{bmatrix}) \\
&= \frac{1}{M\sin\theta_0} h^{\mathrm{T}} \begin{bmatrix} \sin(\theta_1 + \theta_0) - \sin(\theta_1 - \theta_0) \\ \vdots \\ \sin(\theta_M + \theta_0) - \sin(\theta_M - \theta_0) \end{bmatrix} \\
&= \frac{2}{M} h^{\mathrm{T}} \begin{bmatrix} \cos\theta_1 \\ \vdots \\ \cos\theta_M \end{bmatrix} \\
&= \frac{2}{M} h^{\mathrm{T}} n_1
\end{aligned}$$

$$\bar{v}_y = \frac{1}{M} \sum_{i=1}^{M} \frac{1}{\sin\theta_0} \begin{bmatrix} h_i & h_{i+1} \end{bmatrix} \begin{bmatrix} -\cos\theta_{i+1} \\ \cos\theta_i \end{bmatrix}$$

$$= \frac{1}{M\sin\theta_0}(-h^{\mathrm{T}}\begin{bmatrix}\cos\theta_2\\ \cos\theta_3\\ \vdots\\ \cos\theta_M\\ \cos\theta_1\end{bmatrix} + h^{\mathrm{T}}\begin{bmatrix}\cos\theta_M\\ \cos\theta_1\\ \vdots\\ \cos\theta_{M-2}\\ \cos\theta_{M-1}\end{bmatrix})$$

$$= \frac{1}{M\sin\theta_0}h^{\mathrm{T}}\begin{bmatrix}\cos(\theta_1-\theta_0)-\cos(\theta_1+\theta_0)\\ \vdots\\ \cos(\theta_M-\theta_0)-\cos(\theta_M+\theta_0)\end{bmatrix}$$

$$= \frac{2}{M}h^{\mathrm{T}}\begin{bmatrix}\sin\theta_1\\ \vdots\\ \sin\theta_M\end{bmatrix}$$

$$= \frac{2}{M}h^{\mathrm{T}}n_2$$

B. PROOF OF THEOREM 1 (cont.)

To complete the proof, we must show that (6) implies $S_B = S_\nu$. This is done in two stages. First we show that $S_B \subset S_\nu$, then that $S_\nu \subset S_B$. Since S_B is a bounded (convex) polytope (proof omitted), it may be written as

$$S_B = \mathrm{hul}(e_1, e_2, \ldots, e_p) \tag{B.1}$$

where e_i are the extreme points of S_B. Consider one particular extreme point of S_B, e_j; it must satisfy with equality at least two inequalities in (5). Let one of those inequalities be indexed by k. Then we have

$$e_j^{\mathrm{T}}\omega_k = h_k \ , \tag{B.2}$$

i.e., e_j lies on the line L_k. Two of the ν_i's also lie on L_k: ν_{k-1} and ν_k. Now suppose e_j could be written as the convex combination of ν_{k-1} and ν_k. Then any extreme point of S_B

could be written as the convex combination of two points in S_ν. And since both S_B and S_ν are convex, then we must have that $S_B \subset S_\nu$, proving this stage of the theorem.

We now show that e_j can indeed be written as the convex combination of ν_{k-1} and ν_k. Here, there are two possibilities: $\nu_{k-1} = \nu_k$ and $\nu_{k-1} \neq \nu_k$. Each of these cases require some development.

In the case where $\nu_{k-1} = \nu_k$, we show that $e_j = \nu_{k-1} = \nu_k$. First, since e_j and ν_k are on the line perpendicular to ω_k, we may write e_k as

$$e_j = \nu_k + \beta\omega_k^\perp \ , \tag{B.3}$$

where

$$\omega_k^\perp = \begin{bmatrix} 0 & -1 \\ 1 & 0 \end{bmatrix} \omega_k$$

is the perpendicular to ω_k. Taking inner products of both sides of (B.3) with ω_{k-1} and using the fact that e_j is in S_B we may write

$$\omega_{k-1}^{\mathrm{T}} e_j = h_{k-1} + \beta\omega_{k-1}^{\mathrm{T}}\omega_k^\perp \leq h_{k-1}$$

and, similarly, for ω_{k+1}

$$\omega_{k+1}^{\mathrm{T}} e_j = h_{k+1} + \beta\omega_{k+1}^{\mathrm{T}}\omega_k^\perp \leq h_{k+1}$$

Hence,

$$\beta\omega_{k-1}^{\mathrm{T}}\omega_k^\perp \leq 0 \quad \text{and} \quad \beta\omega_{k+1}\omega_k^\perp \leq 0 \ .$$

After simplifying the above expressions using the definitions of ω_{k-1}, ω_{k+1}, and $\omega_k^\perp$, we are led to the contradictory equations

$$\beta(-\sin\theta_0) \leq 0 \quad \text{and} \quad \beta(\sin\theta_0) \leq 0 \ ,$$

hence, β must be zero, and therefore $e_j = \nu_k = \nu_{k-1}$, as required.

In the case where $\nu_{k-1} \neq \nu_k$ we first need an auxiliary result relating the unit vectors ω_{k-1}, ω_k, and ω_{k+1}. From the geometry it is easy to verify that

$$\omega_k = \frac{1}{2\cos\theta_0}\,(\omega_{k-1} + \omega_{k+1}) \tag{B.4}$$

where $\theta_0 = 2\pi/M$. Next, since e_j, ν_{k-1}, and ν_k all lie on the same line L_k, and ν_{k-1} and ν_k are distinct points, we may express e_j as a linear combination of ν_{k-1} and ν_k using the single parameter α as

$$e_j = \alpha\nu_{k-1} + (1-\alpha)\nu_k \tag{B.5}$$

Taking the inner product of both sides of (B.5) with ω_{k-1} we have

$$\begin{aligned} e_j^{\mathrm{T}}\omega_{k-1} &= \alpha\nu_{k-1}^{\mathrm{T}}\omega_{k-1} + (1-\alpha)\nu_k^{\mathrm{T}}\omega_{k-1} \\ &= \alpha h_{k-1} + (1-\alpha)\nu_k^{\mathrm{T}}\omega_{k-1} \\ &\leq h_{k-1} \ . \end{aligned} \tag{B.6}$$

The last inequality results from the fact that e_j is, by definition, in S_B. Now we eliminate ω_{k-1} from (B.6) using (B.4) yielding

$$\alpha h_{k-1} + (1-\alpha)\nu_k^{\mathrm{T}}(2\cos\theta_0\,\omega_k - \omega_{k+1}) \leq h_{k-1}$$

which may be further reduced to

$$(1-\alpha)(2\cos\theta_0\,h_k - h_{k-1} - h_{k+1}) \leq 0 \ . \tag{B.7}$$

Since from (6) the quantity $2\cos\theta_0\,h_k - h_{k-1} - h_{k+1}$ must be non-positive we immediately recognize that $\alpha \leq 1$.

Taking the inner product of both sides of (B.5) with ω_{k+1} and using a similar sequence of steps leading to (B.7) one may show that

$$\alpha(2\cos\theta_0\,h_k - h_{k-1} - h_{k+1}) \leq 0 \tag{B.8}$$

from which we conclude that $\alpha \geq 0$. Hence, we have that $0 \leq \alpha \leq 1$ and, therefore, that e_j is, in fact, a *convex combination* of ν_{k-1} and ν_k. This completes the proof that $S_B \subset S_\nu$.

Now we begin the proof that $S_\nu \subset S_B$. In what follows, we show that $\nu_i \in S_B$ for each $i = 1, \ldots, M$. Since S_B is convex this is sufficient to prove that S_ν is contained in S_B. Accordingly, we intend to show that

$$\nu_i^{\mathrm{T}}[\omega_1\, \omega_2\, \ldots\, \omega_M] \le [h_1\, h_2\, \ldots, h_M] \tag{B.9}$$

for all $i = 1, \ldots, M$. Substituting expressions for ν_i and ω_j $j = 1, \ldots, M$ into (B.9) and simplifying yields

$$\frac{1}{\sin\theta_0}[q_{i1}\, q_{i2}\, \cdots\, q_{iM}] \le [h_1\, h_2\, \ldots\, h_M] \tag{B.10}$$

where $q_{ij} = h_i \sin(\theta_{i+1} - \theta_j) - h_{i+1}\sin(\theta_i - \theta_j)$. Our task is to show that (B.10) is true given $h^{\mathrm{T}}C \le 0$.

Equation (B.10) is true if each term is separately true. Hence, we must show that

$$\frac{1}{\sin\theta_0}\left(h_i \sin(\theta_{i+1} - \theta_j) - h_{i+1}\sin(\theta_i - \theta_j)\right) \le h_j \tag{B.11}$$

for $i = 1, \ldots, M$ (each ν_i) and $j = 1, \ldots, M$ (each term in (B.9)). Because of the rotational symmetry of the problem we may, without loss of generality, choose $j = 1$ and prove that (B.11) is true for $i = 1, \ldots, M$. Since $\theta_i = (i-1)2\pi/M = (i-1)\theta_0$, then for $j = 1$ we may simplify (B.11) to

$$\frac{1}{\sin\theta_0}\left(h_i \sin i\theta_0 - h_{i+1}\sin(i-1)\theta_0\right) \le h_1 \tag{B.12}$$

Denoting the left-hand side of (B.12) by E_i we have for $i = 1$ that

$$E_1 = \frac{1}{\sin\theta_0}\left(h_1 \sin\theta_0 - 0\right) = h_1$$

which satisfies (B.12) trivially. The general expression E_i for $i = 2, \ldots, M$ may be related to E_1 using the relation $h^{\mathrm{T}}C \le 0$ as follows. From (B.12) we have that

$$E_i = \frac{1}{\sin\theta_0}\left(h_i \sin i\theta_0 - h_{i+1}\sin(i-1)\theta_0\right) \ .$$

Using the formula $\sin ia = 2\sin(i-1)a\cos a - \sin(i-2)a$, this becomes

$$\begin{aligned} E_i &= \frac{1}{\sin\theta_0}\left[h_i\left(2\sin(i-1)\theta_0 \cos\theta_0 - \sin(i-2)\theta_0\right) - h_{i+1}\sin(i-1)\theta_0\right] \\ &= \frac{1}{\sin\theta_0}\left[(2h_i\cos\theta_0 - h_{i+1})\sin(i-1)\theta_0 - h_i\sin(i-2)\theta_0\right] \end{aligned} \tag{B.13}$$

Now we notice that the i^{th} constraint in $h^{\mathrm{T}}C \leq 0$ may be written as $2\cos\theta_i\, h_i - h_{i+1} \leq h_{i-1}$. Using this inequality in (B.13) yields

$$E_i \leq \frac{1}{\sin\theta_0}\left[h_{i-1}\sin(i-1)\theta_0 - h_i \sin(i-2)\theta_0\right]$$

which may be reduced to $E_i \leq E_{i-1}$. This is the result that we sought. Now we may conclude that

$$E_M \leq E_{M-1} \leq \ldots \leq E_2 \leq E_1 = h_1$$

which concludes the proof of sufficiency and, hence, the theorem. □

Affiliation of Authors

The authors are with the Laboratory for Information and Decision Systems, Department of Electrical Engineering and Computer Science, Massachusetts Institute of Technology, Cambridge, MA 02139.

Acknowledgement of Financial Support

This research was supported by the National Science Foundation grant ECS-8312921 and the U.S. Army Research Office grants DAAG29-84-K-0005 and DAAL03-86-K-1071. In addition, the work of the first author was partially supported by a U.S. Army Research Office Fellowship.

Footnotes (also appear in text)

1. A vector inequality such as $x^{\mathrm{T}} \leq y^{\mathrm{T}}$ where $x, y \in \mathbb{R}^{\mathrm{n}}$ implies that $x_i \leq y_i$ for $i = 1, \ldots, n$, where x_i and y_i are the i^{th} elements of the vectors x and y respectively.

2. C is a cone because it obeys the usual property of cones: if h is in C then αh $(\alpha > 0)$ is also in C. It is a polyhedron because it is the intersection of a finite number of closed half spaces in $\mathbb{R}^M$.

Index Terms

- Set Reconstruction
- Support Lines
- Computational Geometry
- Constrained Optimization
- Computed Tomography
- Shape Estimation

References

[1] G. T. Herman, *Image Reconstruction from Projections.* New York: Academic Press, 1980.

[2] P. L. Van Hove and J. G. Verly, "A silhouette-slice theorem for opaque 3-d objects," in *Proc. of the IEEE Intl. Conf. on Acoustics, Speech, and Sig. Proc.*, pp. 933–936, IEEE ASSP, March 26–29 1985.

[3] P. L. Van Hove, *Silhoutte Slice Theorems.* PhD thesis, Massachusetts Institute of Technology, Dept. of Electrical Engineering, 1986.

[4] J. L. Prince, "Geometric model-based Bayesian estimation from projections," April 1986. Proposal for Ph.D. research, M.I.T., Dept. of Electrical Engineering.

[5] D. J. Rossi and A. S. Willsky, "Reconstruction from projections based on detection and estimation of objects–parts I and II: performance analysis and robustness analysis," *IEEE Trans. ASSP*, vol. ASSP-32, no. 4, pp. 886–906, 1984.

[6] Y. Bresler and A. Macovski, "Estimation of 3-d shape of blood vessels from x-ray images," in *Proc. IEEE Comp. Soc. Int. Symp. on Medical Images and Icons*, 1984.

[7] J. S. Schneiter, *Automated Tactile Sensing for Object Recognition and Localization.* PhD thesis, Massachusetts Institute of Technology, Dept. of Mechanical Engineering, 1985.

[8] B. K. P. Horn, *Robot Vision.* Cambridge, MA: MIT Press, 1986.

[9] J. M. Humel, *Resolving Bilinear Data Arrays.* Master's thesis, Massachusetts Institute of Technology, Dept. of Electrical Engineering, 1986.

[10] F. P. Preparata and M. I. Shamos, *Computational Geometry.* New York: Springer-Verlag, 1985.

[11] J. Greshak, *Reconstructing Convex Sets.* PhD thesis, Massachusetts Institute of Technology, Dept. of Electrical Engineering, 1985.

[12] L. A. Santalo, *Integral Geometry and Geometric Probability.* Vol. 1 of *Encyclopedia of mathematics and its applications*, Reading MA: Addison-Wesley, 1976.

[13] P. J. Kelly and M. Weiss, *Geometry and Convexity – a Study in Mathematical Methods.* New York: John Wiley and Sons, 1979.

[14] M. Spivak, *A Comprehensive Introduction to Differential Geometry.* Vol. 2, Berkeley: Publish or Perish, Inc., 1979.

[15] J. L. Prince and A. S. Willsky, "Estimation algorithms for reconstructing a convex set given noisy measurements of its support lines," Tech. Rep. LIDS-P-1638, M.I.T. Laboratory for Information and Decision Systems, January 1987.

[16] R. Bellman, *Introduction to Matrix Analysis.* New York: McGraw-Hill, 1970.

[17] H. L. Van Trees, *Detection, Estimation, and Modulation Theory, Part I.* New York: John Wiley and Sons, 1968.

[18] A. H. Land and S. Powell, *Fortran Codes for Mathematical Programming.* London: Wiley-Interscience, 1973.

[19] D. Goldfarb and A. Idnani, "A numerically stable dual method for solving strictly convex quadratic programs," *Mathematical Programming*, vol. 27, pp. 1–33, 1983.

[20] D. G. Luenberger, *Linear and Nonlinear Programming.* Reading MA: Addison-Wesley, 1984.

Figure Captions

Figure 1. The geometry of computed tomography.

Figure 2. A circle with (a) six true support lines, and (b) six noisy measurements.

Figure 3. The geometry of support lines.

Figure 4. For consistency, line L_i must lie to the left of the dotted line.

Figure 5. (a) Inconsistent lines, the sets S_B and S_ν, and the vertex points ν_i. (b),(c) Consistent lines, the sets S_B and S_ν, and the vertex points ν_i.

Figure 6. Three support lines and a face of S_B.

Figure 7. (a) The true object (circle), the measured support vector ($\gamma = 0.2$), and the reconstruction obtained using the intersection method. (b) Closest, (c) Mini-Max, and (d) Close-Min estimates.

Figure 8. (a) The true object (circle), the measured support vector ($\gamma = 0.4$), and the reconstruction obtained from the intersection method. (b) Closest, (c) Mini-Max, and (d) Close-Min estimates.

Figure 9. (a) The true object (ellipse), the measured support vector ($\gamma = 0.2$), and the reconstruction obtained from the intersection method. (b) Closest, (c) Mini-Max, and (d) Close-Min estimates.

Figure 10. (a) The true object (ellipse), the measured support vector ($\gamma = 0.4$), and the reconstruction obtained from the intersection method. (b) Closest, (c) Mini-Max, and (d) Close-Min estimates.

Figure 11. The observation bounds and the Mini-Max estimate.

Figure 12. Shift-corrected Mini-Max estimate.

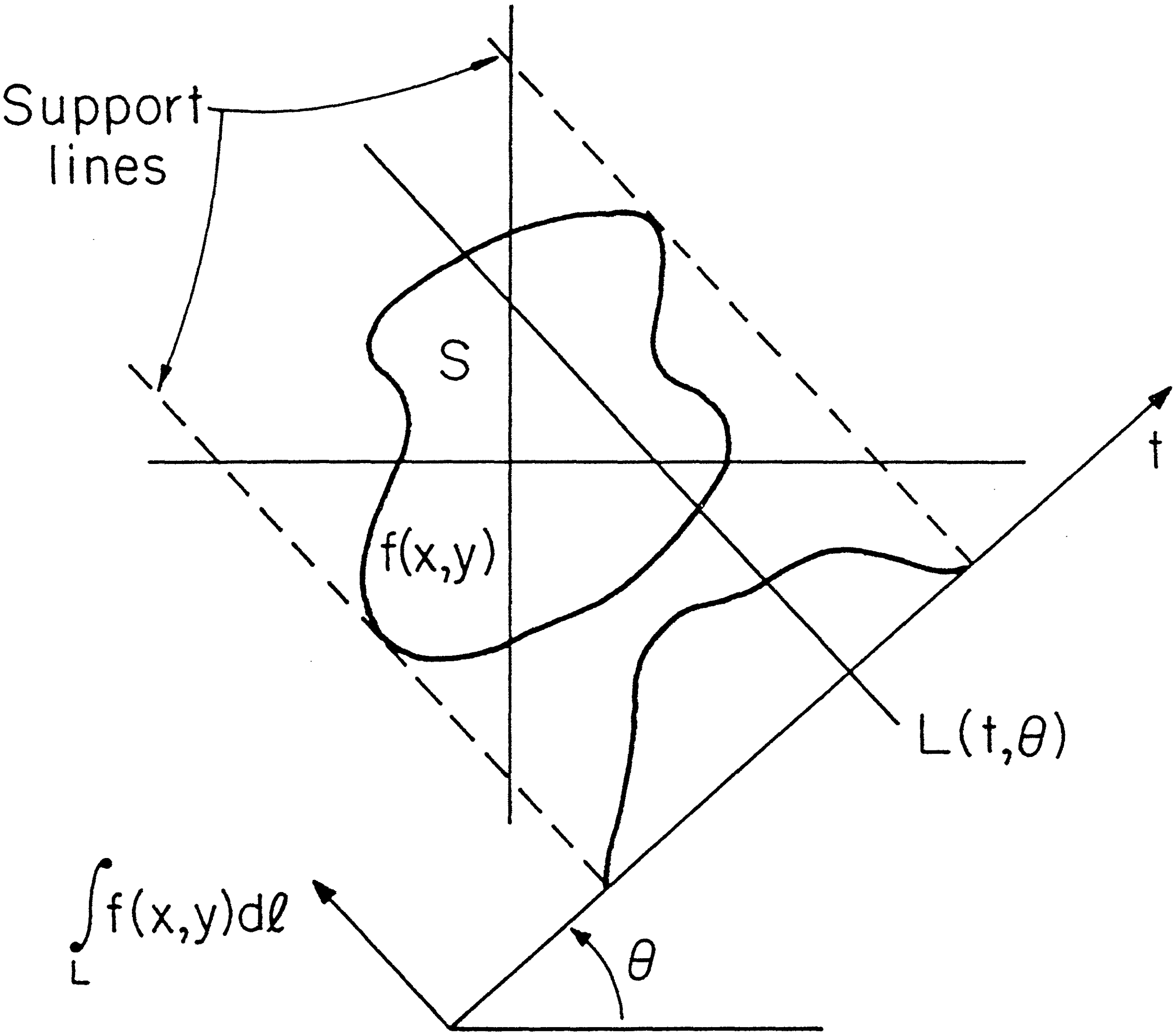

Fig. 1.

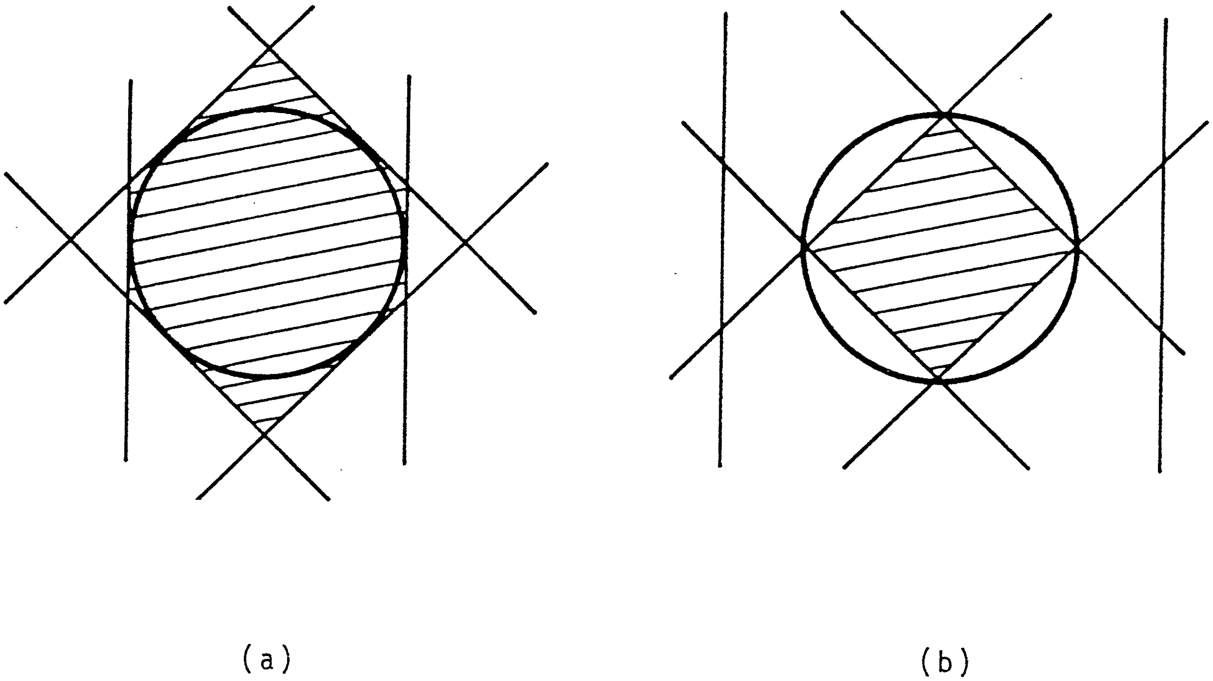

Fig. 2.

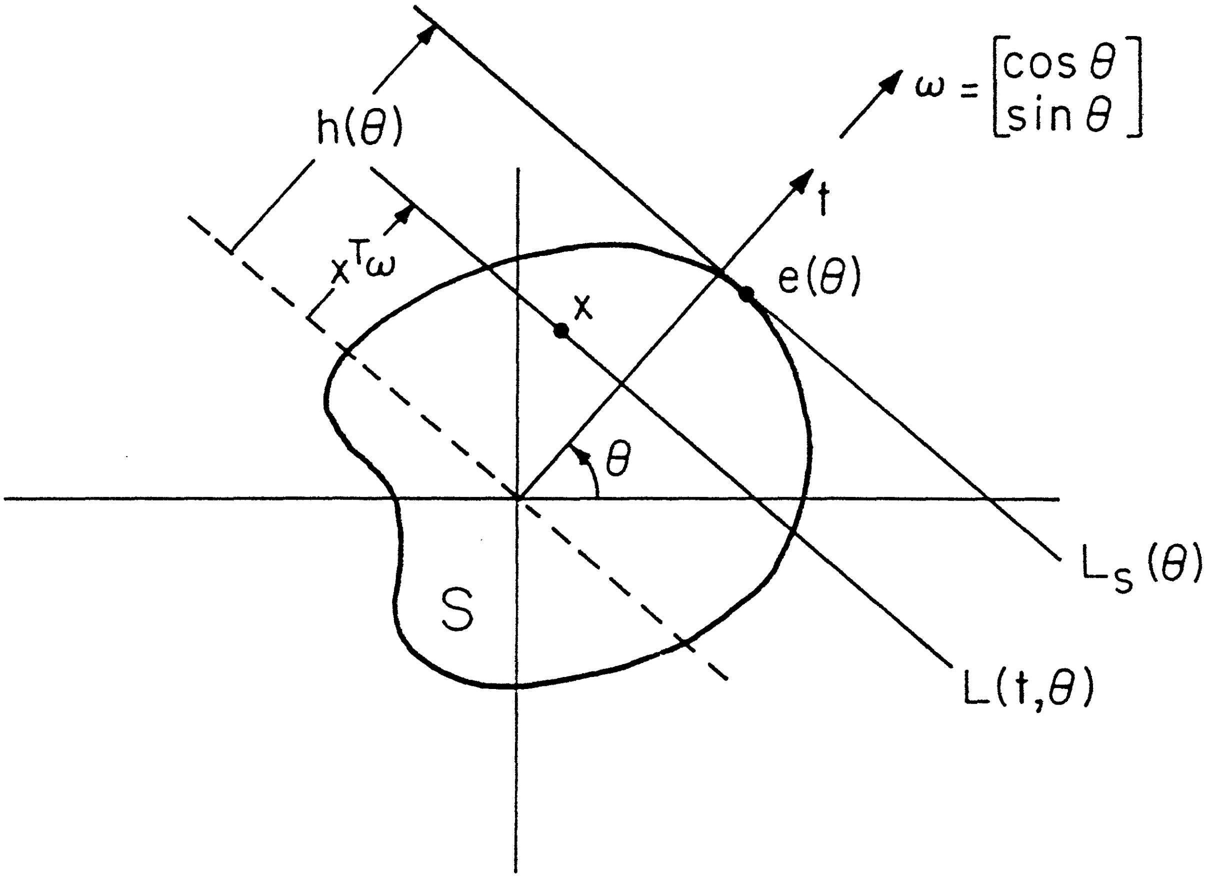
$\omega = \begin{bmatrix}\cos\theta \\ \sin\theta\end{bmatrix}$
$h(\theta)$
t
$x^T\omega$
$e(\theta)$
x
θ
$L_S(\theta)$
S
$L(t,\theta)$

Fig. 3.

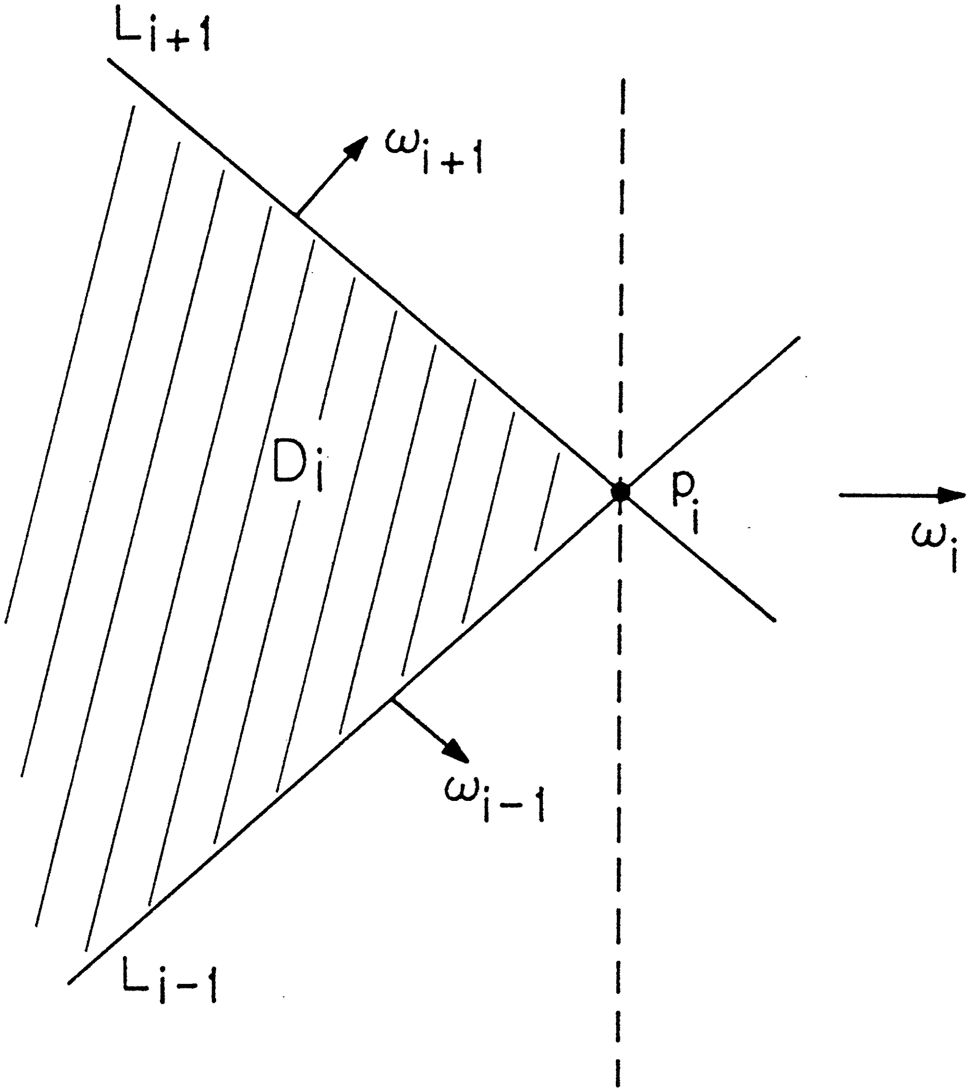

Fig. 4.

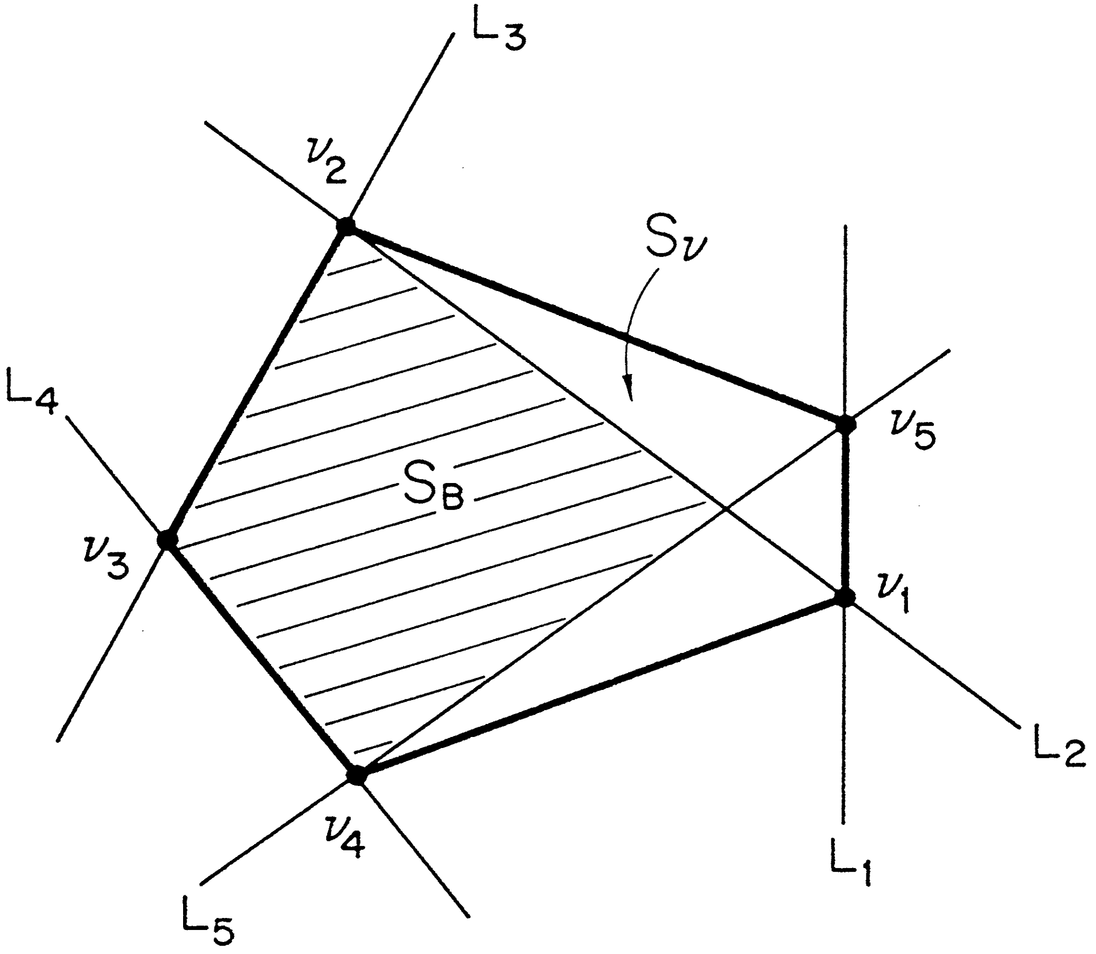

Fig. 5a.

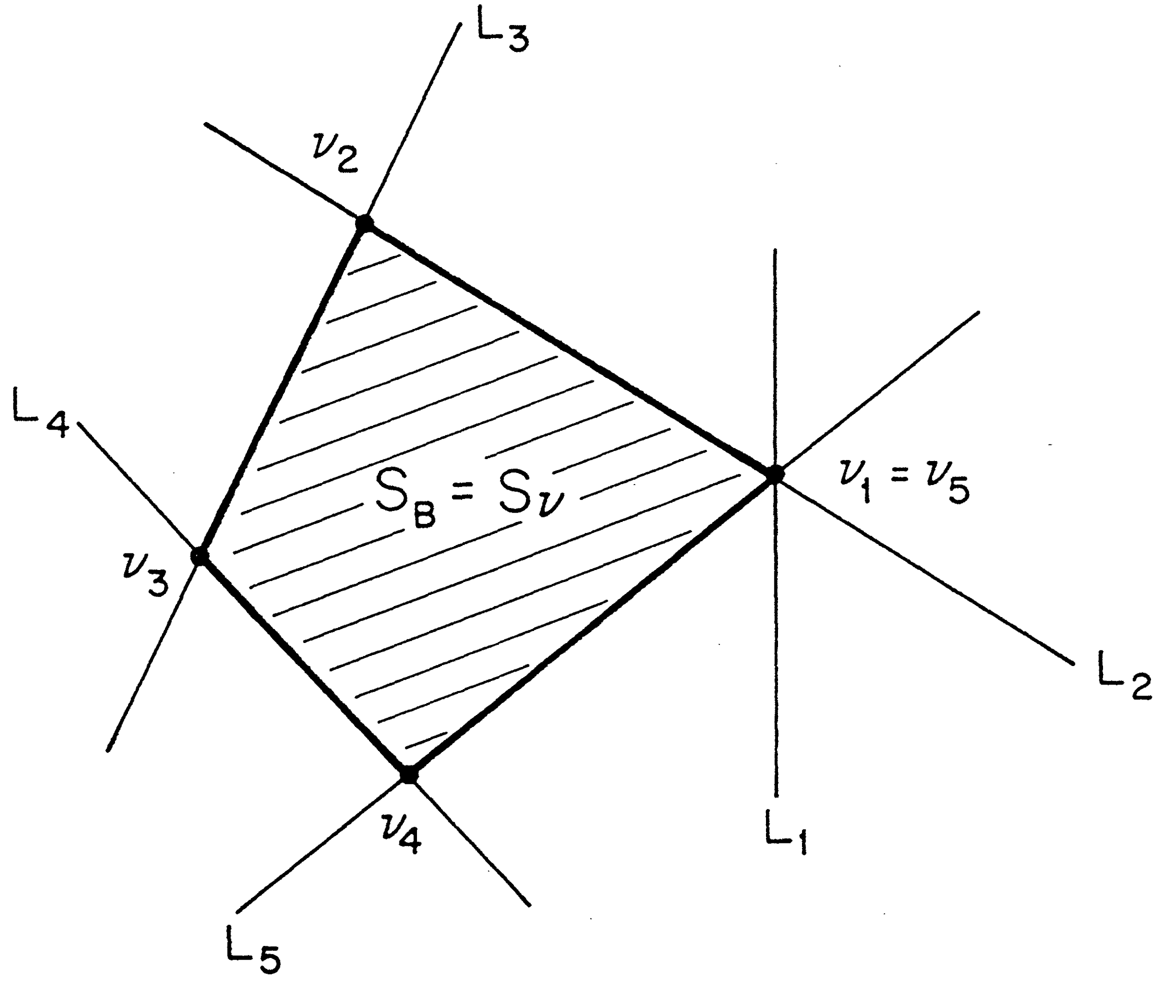

Fig. 5b.

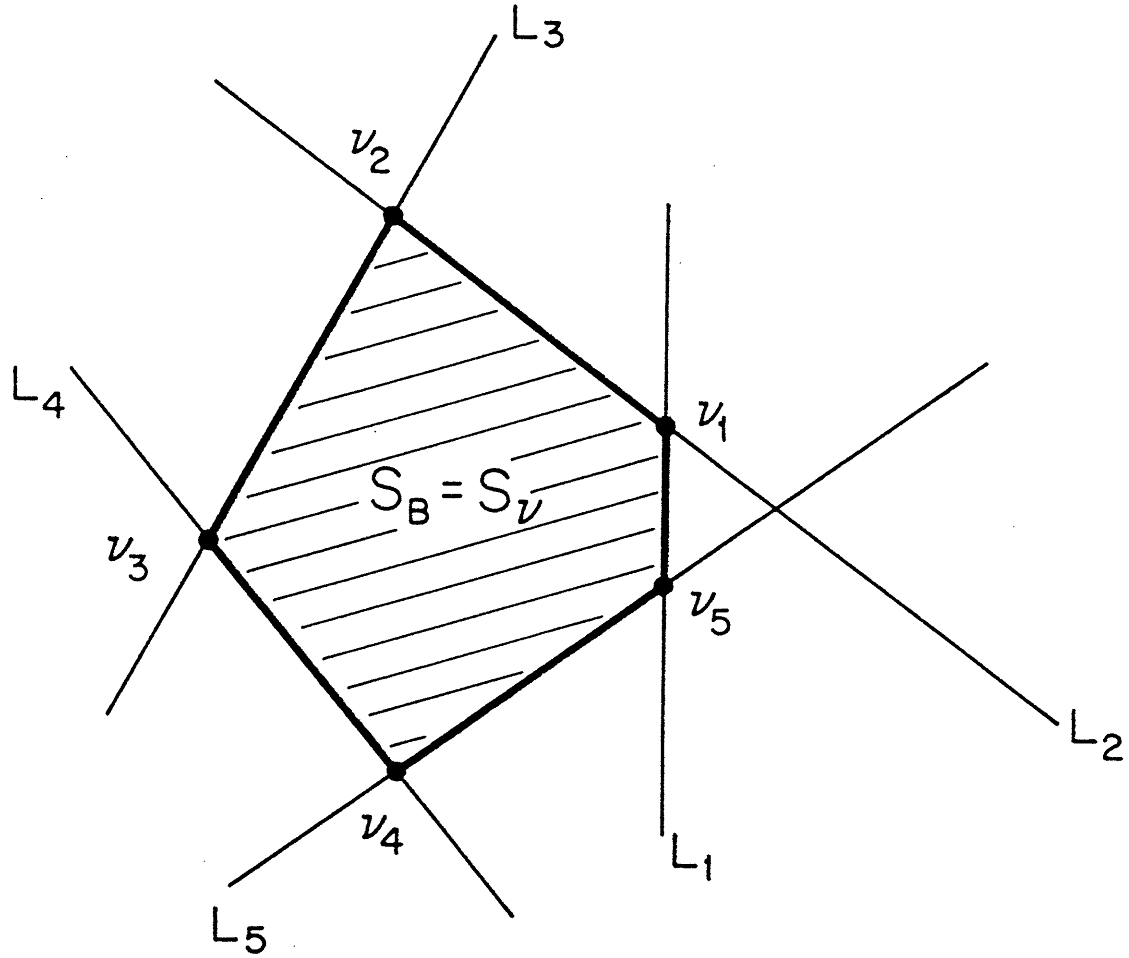

Fig. 5c.

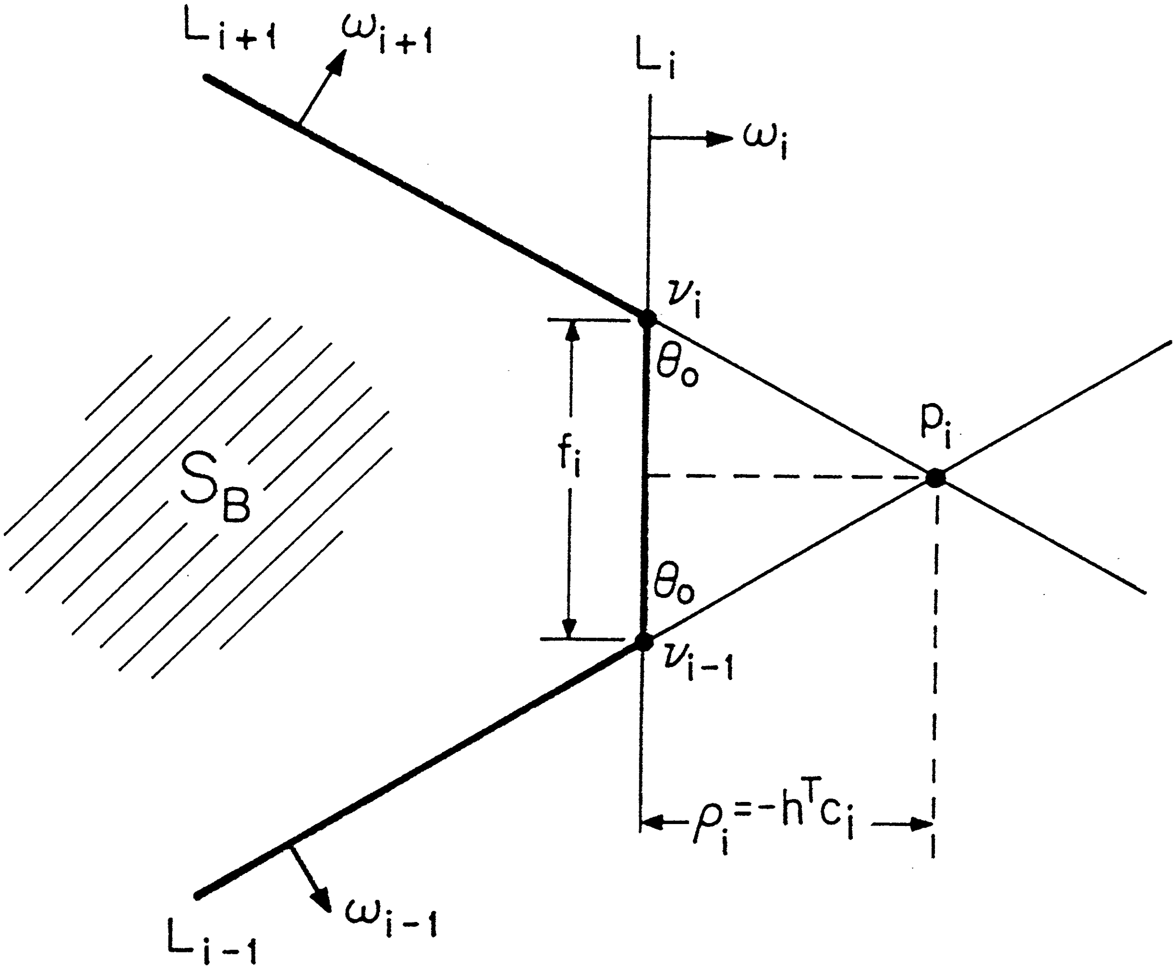
L_{i+1}
ω_{i+1}
L_i
ω_i
ν_i
θ_o
p_i
f_i
S_B
θ_o
ν_{i-1}
$\rho_i = -h^T c_i$
ω_{i-1}
L_{i-1}

Fig. 6.

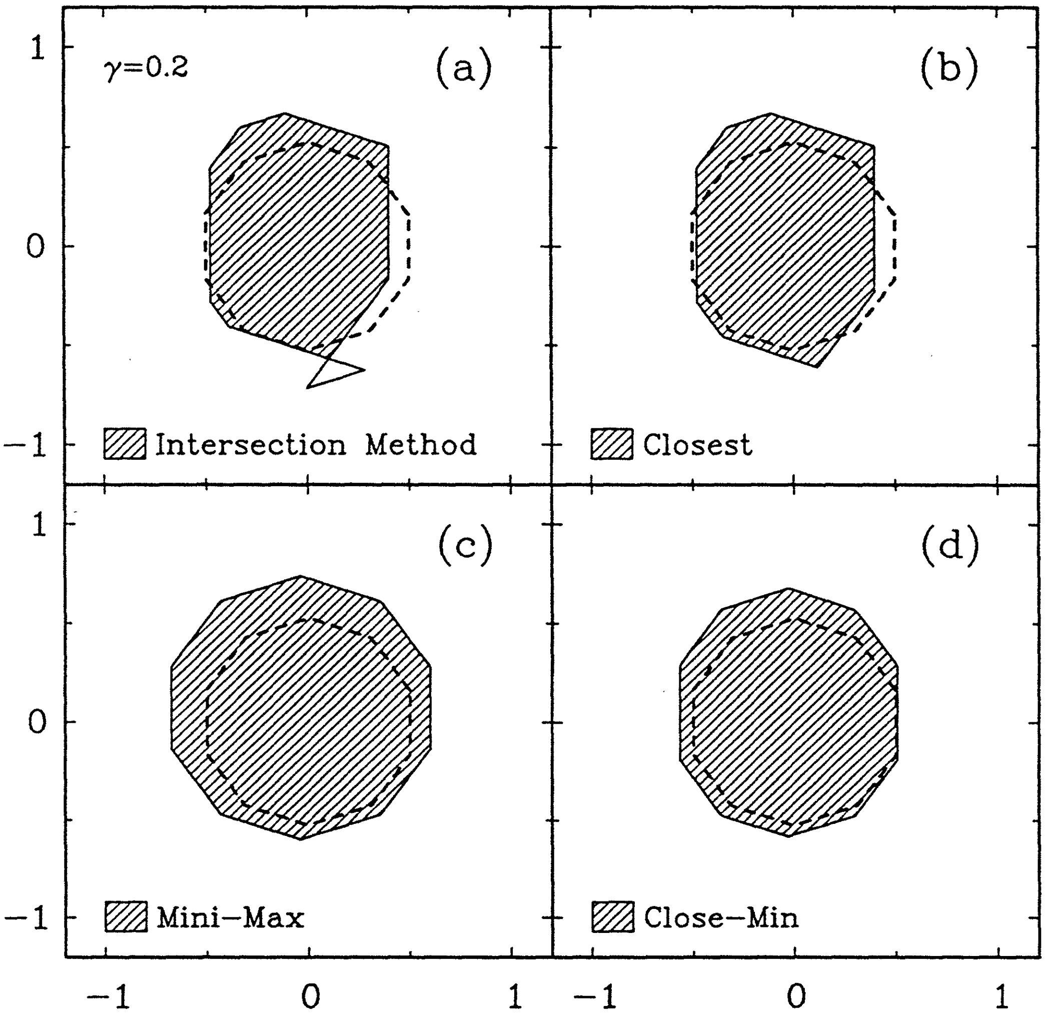
γ=0.2
(a)
(b)
(c)
(d)
▨ Intersection Method
▨ Closest
▨ Mini–Max
▨ Close–Min
1
0
−1
1
0
−1
−1
0
1
−1
0
1

Fig. 7.

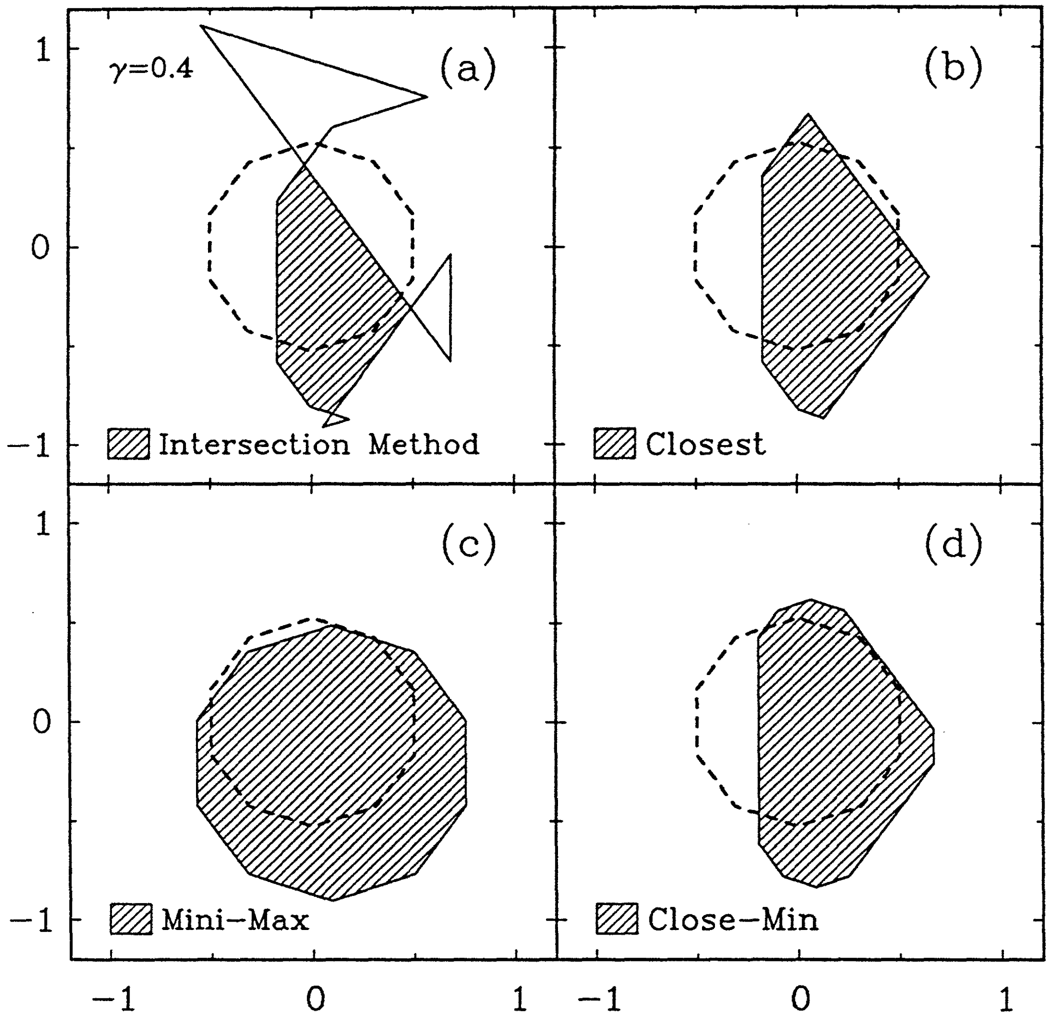
γ=0.4
(a)
(b)
(c)
(d)
▨ Intersection Method
▨ Closest
▨ Mini−Max
▨ Close−Min
1
0
−1
1
0
−1
−1
0
1
−1
0
1

Fig. 8.

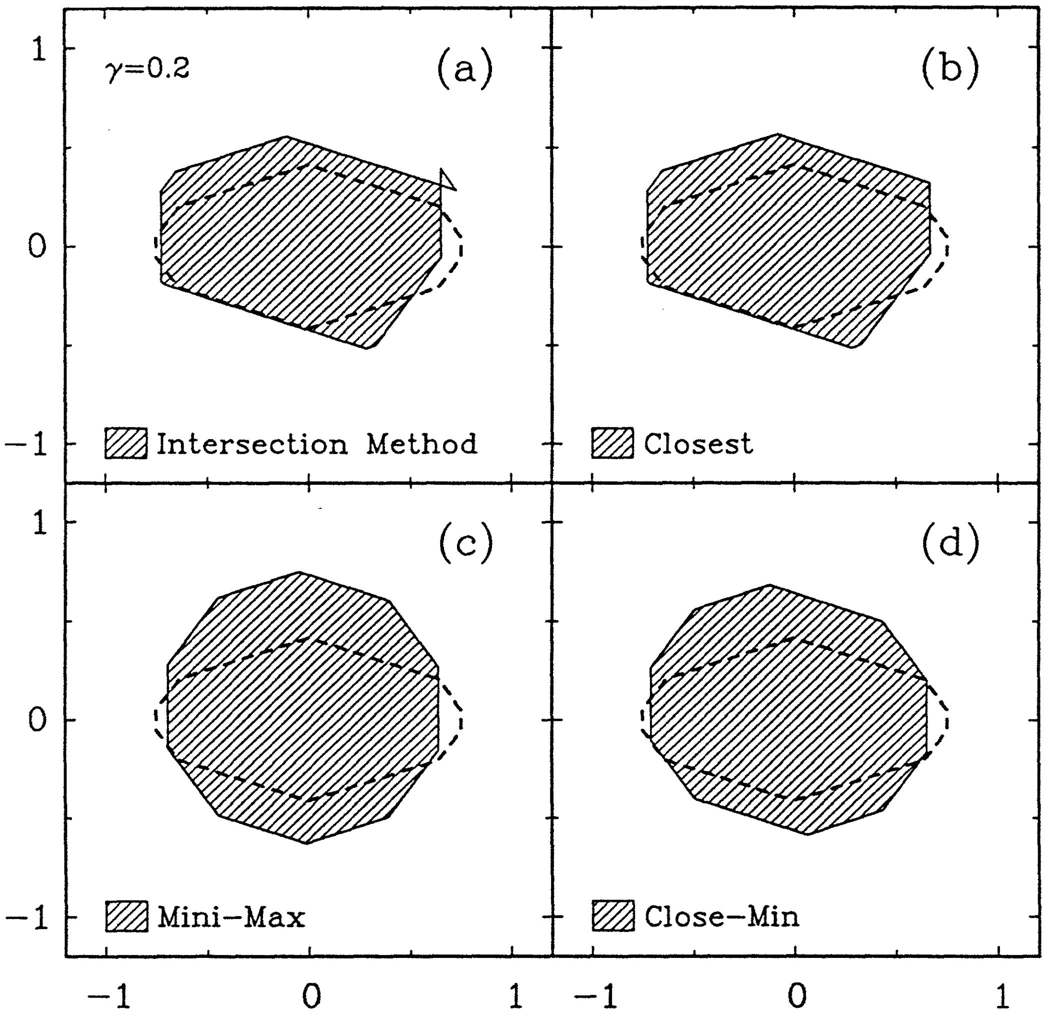
γ=0.2
(a)
(b)
(c)
(d)
▨ Intersection Method
▨ Closest
▨ Mini–Max
▨ Close–Min
1
0
−1
1
0
−1
−1
0
1
−1
0
1

Fig. 9.

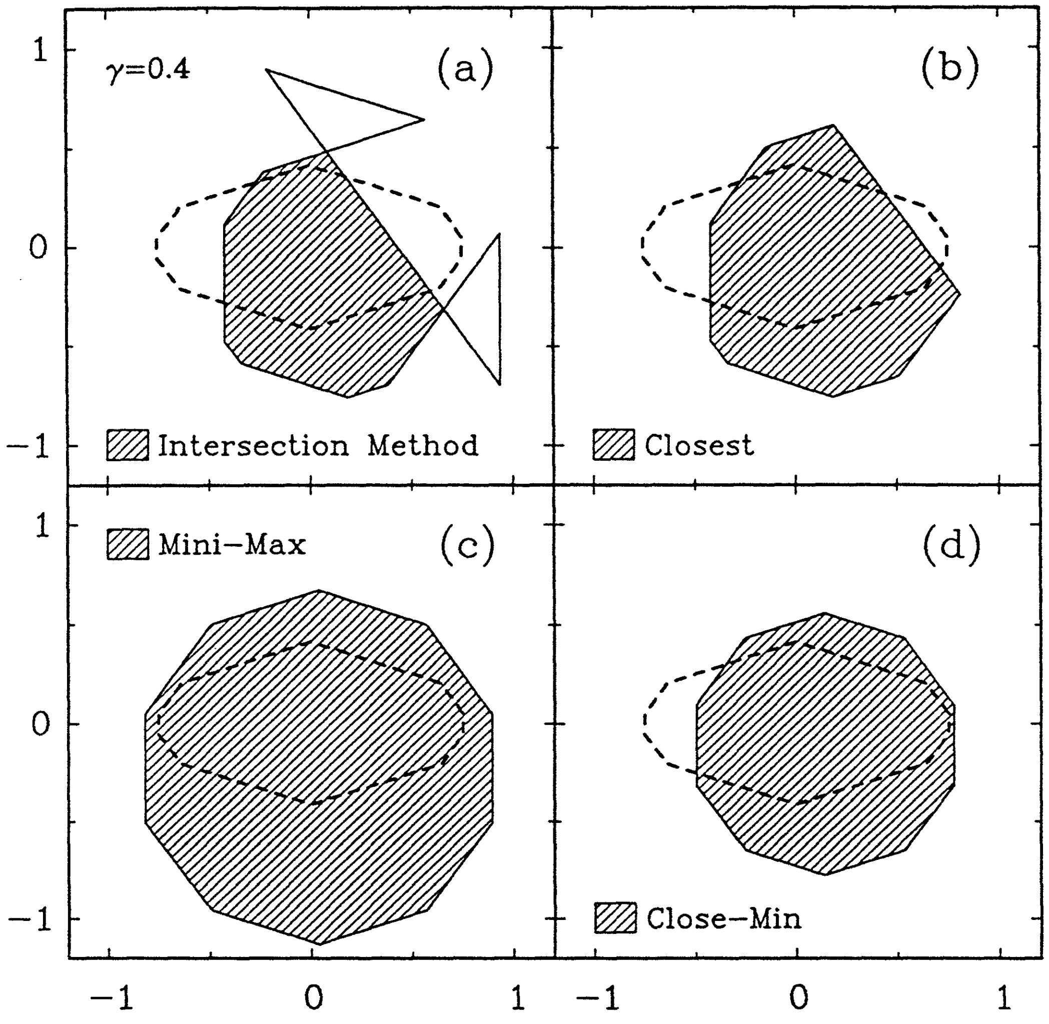
γ=0.4
(a)
▨ Intersection Method
(b)
▨ Closest
▨ Mini–Max
(c)
(d)
▨ Close–Min
1
0
−1
1
0
−1
−1
0
1
−1
0
1

Fig. 10.

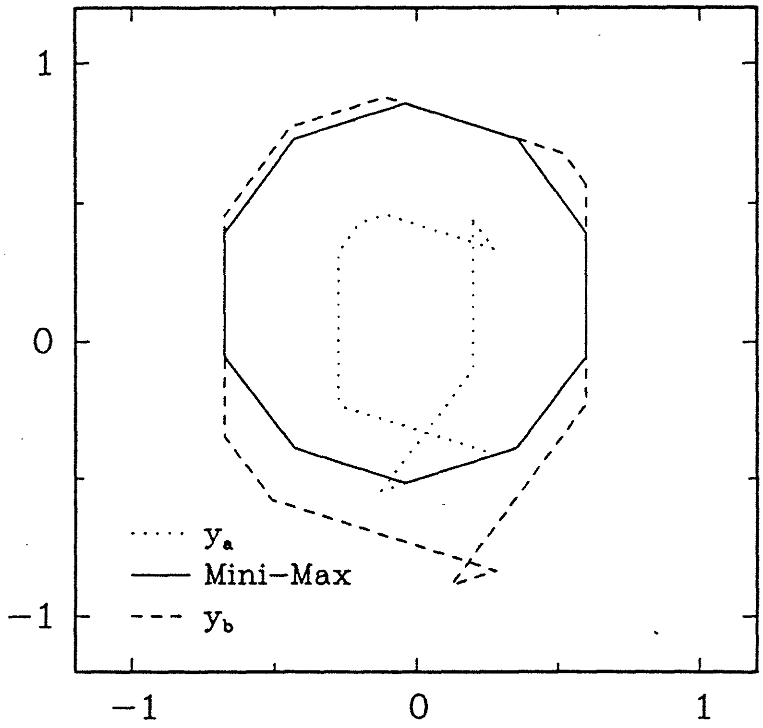

Fig. 11.

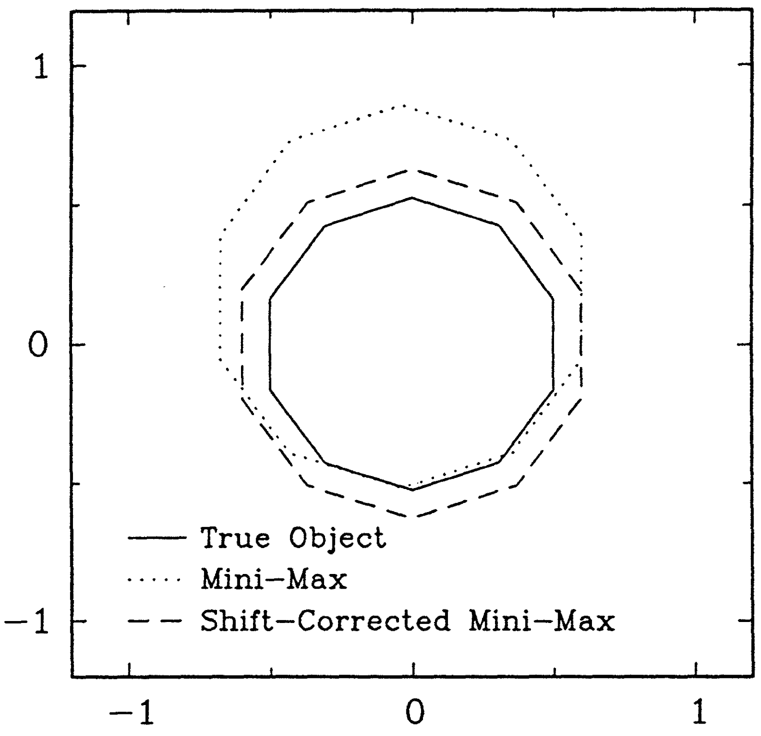

Fig. 12.